PHYSICS REPORTS (Review Section of Physics Letters) 201, No. 5 (1991) 279–334. North-Holland

MICROSCOPIC THEORY OF THE TOTAL REACTION CROSS SECTION AND APPLICATION TO STABLE AND EXOTIC NUCLEI*

M.S. HUSSEIN

Instituto de Física, Universidade de São Paulo, C.P. 20516, 01498 São Paulo, S.P., Brazil

R.A. REGO

Divisão de Física Teórica, Instituto de Estudos Avançados, Centro Técnico Aeroespacial, 12200 São José dos Campos, S.P., Brazil

and

C.A. BERTULANI

Instituto de Física, Universidade Federal do Rio de Janeiro, 21.945 Rio de Janeiro, RJ, Brazil

Editor: G.E. Brown Received October 1990

Contents:

Abstract:

The multiple scattering theory is used to develop a theoretical framework for the calculation of the heavy-ion total reaction cross section. Several important medium effects such as Pauli blocking, are included. The second-order double-scattering contribution to the ion–ion $t\rho_1\rho_2$ interaction is calculated and found to contribute at most an effect of 10% on σ_R. It is found that, whereas at intermediate energies the $t\rho_1\rho_2$ accounts reasonably well for the total reaction cross section, indicating the predominance of single-nucleon knockout at these energies, it underestimates σ_R at lower energies by a large amount. This is mainly due to the absence in $t\rho_1\rho_2$ of fusion and inelastic surface excitation. The case of exotic (neutron- and proton-rich) nuclei is also discussed.

* Supported in part by the CNPq and FAPESP.

0 370-1573/91/$19.60

MICROSCOPIC THEORY OF THE TOTAL REACTION CROSS SECTION AND APPLICATION TO STABLE AND EXOTIC NUCLEI

M.S. HUSSEIN

Instituto de Física, Universidade de São Paulo, C.P. 20516, 01498 São Paulo, S.P., Brazil

R.A. REGO

Divisão de Física Teórica, Instituto de Estudos Avançados, Centro Técnico Aeroespacial, 12200 São José dos Campos, S.P., Brazil

and

C.A. BERTULANI

Instituto de Física, Universidade Federal do Rio de Janeiro, 21.945 Rio de Janeiro, RJ, Brazil

NORTH-HOLLAND

1. Introduction

In recent years the total reaction cross section of heavy ions has become the focus of extensive theoretical [1–6, 64–68] and experimental [7–10, 69, 70] attention. The reaction cross sections also find application in diverse research areas such as radiobiology and space science [71]. On the theoretical side, microscopic calculations have been performed within both the $t\rho_1\rho_2$ [2] Lax approximation and the more exact G-matrix formulation [4]. A major emphasis has been allocated to the discussion of the degree of transparency in the heavy-ion system, and how this is traced to the nucleon–nucleon scattering. A basic input in this calculation is the nucleon–nucleon elastic t-matrix appropriately modified to take into account nuclear medium effects in both projectile and target.

Since at intermediate energies these medium effects can be taken into account as corrections added a posteriori to the free nucleon–nucleon t-matrix, one may use this exhaustively studied object in the calculation of σ_R. Owing to the linear relation involving the total nucleon–nucleon cross section and Im t, through the optical theorem, the energy variation of σ_T^{NN} is accordingly quite relevant for the purpose. In particular the discussion of the reactive content of σ_R, whether for nucleon–nucleus or nucleus–nucleus systems, becomes intimately related to that of σ_T^{NN}.

To set the stage for action we shown in fig. 1 the already extensively exhibited σ_T^{NN} versus center-of-mass energy, for the pp and pn systems [11]. We note that σ_T^{pn} is about twice as large as σ_T^{pp} or σ_T^{nn} at small energies. At intermediate energies they become comparable. Ignoring the very small bremsstrahlung emission, the cross section σ_T^{pn} at $E_{Lab} < 280$ MeV is practically 100% elastic scattering. The first reaction channel, namely one-pion production, opens at $E_{Lab} \sim 280$ MeV, followed at $E_{Lab} = 530$ MeV by the two-pion production cross section, etc. Thus in the energy range 280 MeV $< E_{Lab} <$ 530 MeV the nucleon–nucleon total reaction cross section is just the one-pion production cross section integrated over angle. This is shown in fig. 2.

In fact, what is plotted are the production cross sections for the isospin $T = 1$ and $T = 0$ states. The identifications $\sigma_R(T=1) = \sigma_R^{pp}$ and $\sigma_R(T=0) = 2\sigma_R^{np} - \sigma_R^{pp}$ then give the relevant nucleon–nucleon cross section. As a result, one finds, at least in the energy regime $E_{Lab} < 530$ MeV (i.e., before reaching the two-pion production threshold), that σ^{np} is about 62% of σ_R^{pp}. For the purpose of completeness, we also show, in fig. 3, the two-pion production cross section $\sigma(np \to np\pi^+\pi^-)$ and $\sigma(pp \to pp\pi^+\pi^-)$. These cross sections are orders of magnitude smaller than the one-pion production cross section.

Clearly, the threshold energies for one- and two-pion production processes in the free nucleon–nucleon system are significantly reduced in magnitude in the nucleon–nucleus and more so in the nucleus–nucleus systems, owing to nuclear medium effects, as experimental findings have shown [12]. This fact, however does not necessarily indicate that qualitative considerations concerning the reactive context of nucleon–nucleus ($t\rho$), and nucleus–nucleus ($t\rho_1\rho_2$) interactions, respectively, cannot be made using as a guideline the nucleon–nucleon reaction cross sections discussed so far.

Accordingly we can afirm that the reactive content of the $t\rho$ and $t\rho_1\rho_2$ interaction is predominantly single-nucleon knockout [13] at low energies, and/or one- or two-pion production at intermediate energies. Clearly the excitation of collective degrees of freedom is not accounted for in either of the interactions mentioned above. Thus it becomes quite important to investigate the energy range in which the $t\rho_1\rho_2$ interaction is the dominant component of the ion–ion potential.

The vehicle through which the above can be accomplished is the multiple-scattering description. This theory, not only supplies a convenient framework through which the simple Lax potential can be derived and discussed, but it also makes possible the construction of higher-order corrections which may contribute significantly to σ_R at lower energies.

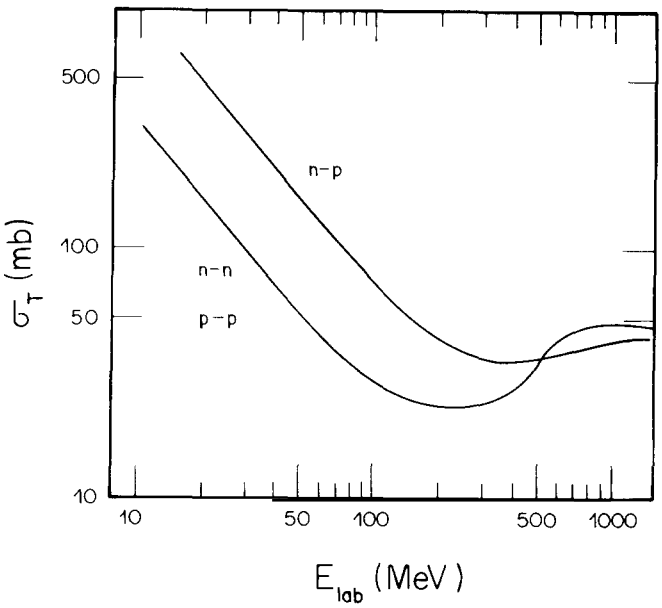

Fig. 1. The total cross section of the NN system versus laboratory energy (from ref. [11]).

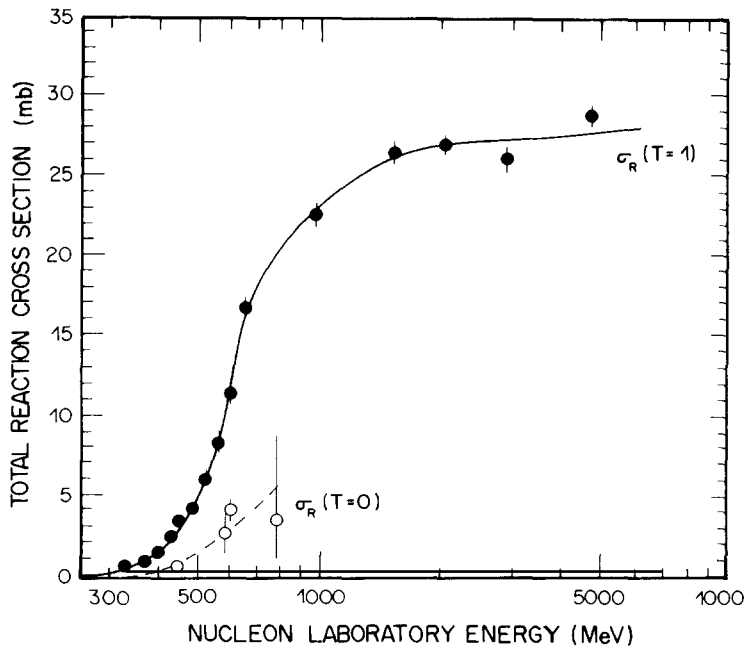

Fig. 2. The angle-integrated one-pion production cross section for the NN system (from ref. [11]).

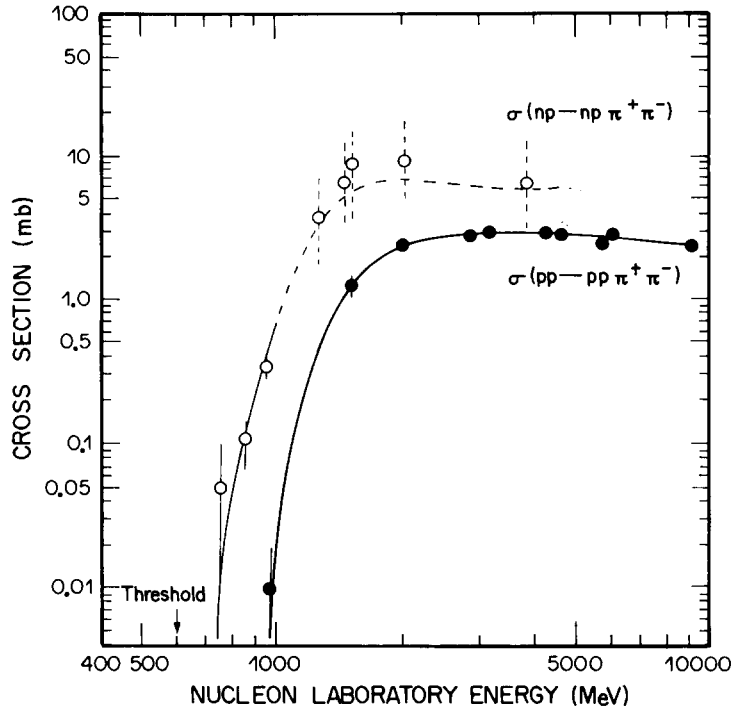

Fig. 3. The angle-integrated two-pion production cross section for the NN system (from ref. [11]).

It is the purpose of this report to investigate the significance of the $t\rho_1\rho_2$ interaction for the total reaction cross section of heavy ions. Both nuclear medium effects and higher-order, multiple-scattering contributions, are discussed. The principal aim is to delineate the energy range in which this interaction (at least its reactive content) approximates well the interaction beftween two nuclei. Recent studies [2], have suggested that even at low energies ($E < 15$ MeV/N) the $t\rho_1\rho_2$ interaction reproduces well the total reaction cross section. As we shall see later in this report this is not so on account of the fact that several important reaction channels, not accounted for by the $t\rho_1\rho_2$ potential, whose major reactive channel is single-nucleon knockout in both projectile and target nuclei, become increasingly important as the energy is lowered.

The organization of this report is as follows: in chapter 2 we present a detailed account of the theory of σ_R. In particular we discuss several approximations used for its evaluation. We also generalize the one-channel theory of σ_R to multichannels. In chapter 3 we present a summary of the multiple-scattering theory appropriate to heavy-ion collisions. The first-order $t\rho_1\rho_2$ interaction as well as the second-order double-scattering contributions are then derived and analyzed. The imaginary part of the $t\rho_1\rho_2$ interaction is then fully discussed in chapter 4. A very careful analysis of the Pauli blocking in the context of heavy ions is also presented in this chapter. Further, we assess the importance of using a relativistic Dirac formalism in the calculation of σ_R. Calculations of σ_R for several HI systems is then presented in chapter 5, with a comparison with the data made for $^{12}C + ^{12}C$. The effect of the identity of the particles on σ_R is also discussed.

The role of peripheral processes, with the collective participation of several nucleons on the mutual excitation of the nuclei, is discussed in chapter 6. Of great interest in this context is the excitation of

giant resonances in intermediate and high energy collisions, which reveal new aspects of the nuclear structure not accessible by means of other nuclear probes. As we show later, the peripheral processes imply a very peculiar mode of absorption of energy by the nuclei. The absorption of energy in peripheral collisions at high energies will go preferentially to the excitation of collective motions or to emission of a pair of nucleons, or clusters. As a brief account of this subject, we shall particularly direct our attention to the reactions with radioactive secondary beams, which is a subject of increasing interest. Finally, in chapter 7, our concluding remarks are presented.

A number of appendices relevant for the discussion presented in the different chapters of the report are collected at the end.

2. Theory of the total reaction cross section

In this section we present the full details of the theoretical structure of the total reaction cross section. The basic relation between σ_R and the imaginary part of the optical potential is most generally and easily obtained using the generalized optical theorem. This we do first. We then turn to the discussion of σ_R within several limiting cases and approximations, in particular we investigate the eikonal expression for σ_R.

Let us first consider the Lippmann–Schwinger equation for the optical T-matrix which describes elastic scattering

$$T = V + VG_0^{(+)}(E)T\,, \tag{2.1}$$

where $G_0^{(+)}$ is the free propagator or Green function, $(E - H_0 + i\varepsilon)^{-1}$, with H_0 being the free Hamiltonian. In eq. (2.1), V denotes the complex optical potential.

We multiply eq. (2.1) from the right by T^{-1} and from left by V^{-1} to obtain

$$V^{-1} = T^{-1} + G_0^{(+)}(E)\,. \tag{2.2}$$

Applying the same procedure for the complex conjugate version of (2.1) gives

$$V^{\dagger(-1)} = T^{\dagger(-1)} + G_0^{(-)}(E)\,. \tag{2.3}$$

Subtracting (2.3) from (2.2) results in

$$T^{-1} - T^{\dagger(-1)} = V^{-1} - V^{\dagger(-1)} + 2\pi i\delta(E - H_0)\,. \tag{2.4}$$

The last term in eq. (2.4) is just the difference $G_0^{(+)}(E) - G_0^{(-)}(E)$. We now multiply eq. (2.4) from the left by $T^\dagger$ and from the right by T to get, after using the relations $T = V\Omega^{(+)}$ and $T^\dagger = \Omega^{(+)\dagger}V^\dagger$ where $\Omega^{(+)}$ is the Möller wave operator,

$$T - T^\dagger = \Omega^{(+)\dagger}(V - V^\dagger)\Omega^{(+)} - 2\pi i T^\dagger\delta(E - H_0)T\,. \tag{2.5}$$

We are now in a position to derive the optical theorem which relates the imaginary part of the forward scattering amplitude to the total cross section. Indeed, taking the on-shell matrix element (in

plane waves) of (2.5) leads, immediately to ($k' = k$)

$$\text{Im}\, T^{\text{on-shell}}(k, 0°) = \frac{1}{2\text{i}} \langle k|\Omega^{(+)\dagger}(V - V^{\dagger})\Omega^{(+)}|k'\rangle - \frac{1}{2\text{i}} \frac{2\pi\text{i}\mu k}{(2\pi)^3\hbar^2} \int \text{d}\Omega_k \, |T^{\text{on-shell}}_{(k',k,\hbar k^2/2\mu)}|^2 . \tag{2.6}$$

Using now the relation between $T^{\text{on-shell}}$ and the elastic scattering amplitude f,

$$f(k, \theta) = -(\mu/2\pi\hbar^2) T^{\text{on-shell}}(k, \theta) , \tag{2.7}$$

we obtain

$$\frac{4\pi}{k} \text{Im}\, f(k, 0) = \frac{k}{E_k} \langle \psi_k^{(+)}|\text{Im}\, V|\psi_k^{(+)}\rangle + \int \text{d}\Omega \, |f(k, \theta)|^2 , \tag{2.8}$$

which is the generalized optical theorem we are seeking. Since on the right-hand side, we have the total cross section, and $\int \text{d}\Omega \, |f(k, \theta)|^2$ is the angle-integrated elastic cross section, we can immediately identify the first term on the right-hand side to be just the total reaction cross section

$$\sigma_{\text{R}} = (k/E_k)\langle \psi_k^{(+)}|\text{Im}\, V|\psi_k^{(+)}\rangle . \tag{2.9}$$

In the above derivation of σ_{R} through the use of optical theorem, we did not pay attention to the long-range Coulomb interaction. This, however, poses no fundamental problem as one can generalize the optical theorem, in such a way as to have $\text{Im}[f(0) - f_{\text{Ruth}}(0)]$ on the left-hand side of eq. (2.8) and $\int \text{d}\Omega \, [|f(k, \theta)|^2 - |f_{\text{Ruth}}(k, \theta)|^2]$ as the second term on the right-hand side of the same equation. In the above expressions, $f_{\text{Ruth}}(k, \theta)$ is the Rutherford scattering amplitude. The first term, namely σ_{R} [see eq. (2.9)], is unchanged. For full details of the above generalization we refer the reader to Haldeman and Thaler [14] and Hussein et al. [15]. For completeness, an alternative, more direct, derivation of σ_{R} using the usual Wronskian argument is presented in appendix I.

Equation (2.9) can be straightforwardly expanded in partial waves yielding

$$\sigma_{\text{R}} = \frac{\pi}{k^2} \sum_{l=0}^{\infty} (2l + 1) T_l , \tag{2.10}$$

with the elastic-channel transmission coefficients T_l, given by

$$T_l = \frac{8\mu k}{\hbar^2} \int_0^{\infty} \text{d}r \, |\psi_l(k, r)|^2 |\text{Im}\, V(r)| , \tag{2.11}$$

where $\psi_l(k, r)$ is the partial wave, radial, wave function, which is a solution of the radial optical Schrödinger equation (with the full V). Of course, the following relation holds between T_l and the elastic S-matrix

$$T_l = 1 - |S_l|^2 . \tag{2.12}$$

In the large-number limit of partial waves, and under semiclassical conditions, one may replace the partial-wave sum by an integral and l by $kb - 1/2$, with b being the impact parameter. Thus eq. (2.10) becomes

$$\sigma_R = 2\pi \int_0^\infty b\, db\, T(b)\,. \tag{2.13}$$

In the application to heavy-ion reactions, it has been customary to introduce a strong absorption radius R_{sa} which would limit the b-integral above in the sense that $T(b)$ is represented as

$$T(b) = \Theta(R_{sa} - b)\,. \tag{2.14}$$

Equation (2.14) implies that the limit of infinite absorption (large $\mathrm{Im}\, V$) for $b < R_{sa}$ and zero absorption for $b > R_{sa}$ is a case hardly exactly met in physical systems. It does, however, constitute a reasonable first approximation for $T(b)$. It is important here to remind the reader that R_{sa} is energy dependent, to account for the Coulomb barrier restriction. Usually R_{sa} is taken to be

$$R_{sa} = R_B(1 - V_B/E)^{1/2}\,, \tag{2.15}$$

where R_B and V_B are the position and height of the Coulomb barrier, and E is the center-of-mass energy. With (2.15), σ_R becomes

$$\sigma_R = \pi R_B^2(1 - V_B/E)\,. \tag{2.16}$$

The above expression for σ_R, does account well for heavy-ion total reaction cross-section data up to a center-of-mass energy per nucleon about one fourth the Fermi energy ($\varepsilon_F = 37$ MeV). At higher energies, the data start dropping off until an energy per nucleon of about 140 MeV (roughly equal to the pion rest mass) is reached, after which σ_R rises again. This fact clearly shows that a great amount of transparency is attained at intermediate energies, and the question arises as to how to relate the transparency to more fundamental physical quantities, such as the nucleon–nucleon total cross section. The vehicle through which this is accomplished is the explicit connection between $T(b)$ of eq. (2.13) and the elastic-channel optical potential, as eq. (2.11) implicitly dictates. The optical potential itself is constructed from multiple-scattering theory as will be discussed in section 3.

In terms of the complex phase shift which specifies S, namely $S = \exp(2i\delta)$, we may write

$$T(b) = 1 - \exp[-4\delta_I(b)]\,, \tag{2.17}$$

where $\delta_I(b) = \mathrm{Im}\, \delta(b)$. Within the JWKB approximation, we have for the phase shift

$$\delta_l = \lim_{r\to\infty}\left[\int_{r_1}^{r} dr' \left(k^2 - \frac{l(l+1)}{r'^2} - \frac{2\mu}{\hbar^2} V(r')\right)^{1/2} - \int_{r_0}^{r} dr' \left(k^2 - \frac{l(l+1)}{r'^2}\right)^{1/2}\right], \tag{2.18}$$

where r_1 is the turning point, and $r_0 \equiv (l + \frac{1}{2})/k = b$. The imaginary part of δ_l is obtained immediately,

$$\delta_{\mathrm{I}}(l) = \int_{r_1}^{\infty} \mathrm{d}r' \left[\left(k^2 - \frac{l(l+1)}{r'^2} - \frac{2\mu}{\hbar^2} \operatorname{Re} V(r') \right)^2 + \left(\frac{2\mu}{\hbar^2} \operatorname{Im} V(r') \right)^2 \right]^{1/4} \times \sin[\theta(r')/2] , \tag{2.19}$$

where

$$\tan\theta(r') = -\frac{2\mu}{\hbar^2} \operatorname{Im} V(r') \left(k^2 - \frac{l(l+1)}{r'^2} - \frac{2\mu}{\hbar^2} \operatorname{Re} V(r') \right)^{-1} . \tag{2.20}$$

At sufficiently high energies, in the sense of $V/E \ll 1$, one may expand (2.19) to first order in Im V, to obtain

$$\delta_{\mathrm{I}} = -\frac{1}{2} \frac{2\mu}{\hbar^2} \int_{r_1}^{\infty} \mathrm{d}r' \frac{\operatorname{Im} V(r')}{[k^2 - l(l+1)/r'^2 - (2\mu/\hbar^2) \operatorname{Re} V(r')]^{1/2}} , \tag{2.21}$$

which may be considered as a precursor of Glauber (or the eikonal) formula, since with the use of cylindrical coordinates $r' = (z', b)$ and ignoring Re $V(r')$ in the square root, one may write

$$\delta_{\mathrm{I}}(b) = -\frac{1}{4} \frac{2\mu}{\hbar^2 k} \int_{-\infty}^{\infty} \mathrm{d}z' \operatorname{Im} V(\sqrt{b^2 + z'^2}) . \tag{2.22}$$

The above expression is to be contrasted with that given in eq. (2.21), in that the former involves a free trajectory for the incident particle (using classical language) whereas the latter moves on a trajectory determined by the combined Coulomb plus Re $V(r)$ potentials.

We note that $\delta_{\mathrm{I}}(b)$ should behave as a function of impact parameter, similarly to Im $V(b)$. In fact, if we make the approximation Im $V = -W_0 \Theta(R - r')$, we obtain

$$\delta_{\mathrm{I}}(b) = (k/2E) W_0 \sqrt{R^2 - b^2} \Theta(R - b) . \tag{2.23}$$

The difference between expression (2.23) and that obtained with a Wood–Saxon form for Im V is concentrated at the surface region. The transmission coefficient $T(b)$ in eq. (2.17) is then given by

$$T(b) = 1 - \exp[-(2kW_0/E)\sqrt{R^2 - b^2}] . \tag{2.24}$$

It is clear from the above formula that the dependence of $T(b)$ on E and consequently that of σ_{R} is determined from the dependence of W_0 on E. If $W_0 \propto E^{1/2}$, the energy dependence of $T(b)$ is washed out. On the other hand, if $W_0 \propto E^{1/2} \sigma_{\mathrm{NN}}(E)$, then the energy dependence of $T(b)$ is exclusively determined by the energy dependence of $\sigma_{\mathrm{NN}}(E)$, as will be fully discussed later. Obviously, the above simple rule changes as the energy is lowered, since an extra energy dependence will emerge from the factor

$$[k^2 - l(l+1)/r^2 - (2\mu/\hbar^2) \operatorname{Re} V(r)]^{-1/2}$$

in eq. (2.21). Further, nuclear medium effects, e.g. Pauli blocking, introduce a further energy dependence. These questions will be fully addressed in the next section.

Though very schematic, the expression obtained for $T(b)$ in eq. (2.24) using the square well model for Im $V(r)$, still serves to exhibit several interesting features of σ_R. Using eq. (2.24) in eq. (2.13), we obtain for $\sigma_R(E)$

$$\sigma_R(E) = \pi R^2\left(1 - 2\,\frac{1-(1+2R/\lambda)\,e^{-2R/\lambda}}{(2R/\lambda)^2}\right), \tag{2.25}$$

where $\lambda = E/kW_0$ is the mean free path. The equation was first derived by Bethe [16]. To correct for the Couloumb barrier effect one merely replaces (2.25) by [17]

$$\sigma_R(E) = \pi R_E^2\left(1 - 2\,\frac{1-(1+2R_E/\lambda)\,e^{-2R_E/\lambda}}{(2R_E/\lambda)^2}\right)\left(1 - \frac{V_B}{E}\right), \tag{2.26}$$

where $R_E = R + 1/k$.

Equation (2.26) may be compared with the purely geometrical formula (2.16), and thus the transparency factor, T, defined by

$$\sigma_R = \pi R_E^2(1-T)(1-V_B/E)\,, \tag{2.27}$$

can be immediately extracted,

$$T = 2[1-(1+2R_E/\lambda)\,e^{-2R_E/\lambda}](2R_E/\lambda)^{-2}\,. \tag{2.28}$$

Figure 4 exhibits the behaviour of T versus $2R_E/\lambda$.

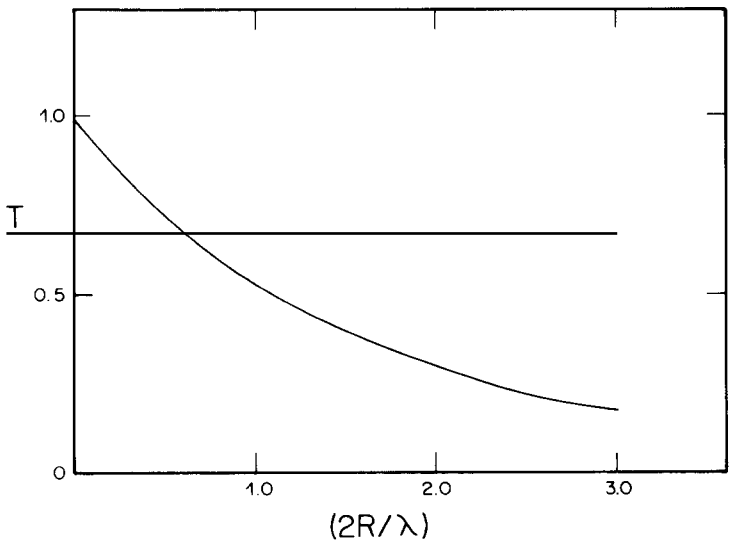

Fig. 4. The transparency factor versus $2\lambda/R$ (eq. 2.28).

Equation (2.28) identifies the physical parameter that determines the value of T, namely $2R_E/\lambda$. For large $2R_E/\lambda$, namely $\lambda \ll 2R_E$, we obtain for T,

$$T \approx \lambda^2/2R_E^2 , \tag{2.29}$$

and accordingly, the total reaction cross section becomes proportional to the surface,

$$\sigma_R \sim \pi R_E^2(1-\lambda^2/2R_E^2)(1-V_B/E)$$
$$\propto \begin{cases} A^{2/3} & \text{for nucleon-induced reaction ,} \\ (A_1^{1/3}+A_2^{1/3})^2 & \text{for ion–ion collisions .} \end{cases} \tag{2.30}$$

The above result is characteristic of strongly interacting systems characterized by short λ such as hadron–nucleus. On the other hand, in the other extreme, namely $2R_E/\lambda \ll 1$ (implying long mean free path λ compared to the effective diameter of the interacting system), we obtain

$$T \approx 1 - \tfrac{2}{3}(2R_E/\lambda) , \tag{2.31}$$

thus giving for the total reaction cross section the following form which is proportional to the effective volume of the system:

$$\sigma_R \sim (\tfrac{4}{3}\pi R_E^3)/\lambda \propto \begin{cases} A & \text{for a nucleon-induced reaction ,} \\ (A^{1/3}+A_2^{1/3})^3 & \text{for ion–ion collisions .} \end{cases} \tag{2.32}$$

The behaviour of σ_R with respect to A in eq. (2.32) is typical of weakly interacting probes with a nuclear target. Examples are electron- and photon-induced reactions. The mean free path in these cases is quite long owing to the weakness of the underlying electromagnetic interaction. Accordingly, the whole nucleus is "seen" in the process of the collision, in contrast to hadron-induced reactions, where only the surface nucleons participate in the collision process.

Clearly, the above picture depends on energy, in the sense that weakly interacting probes behave, at higher energies, like hadrons (in the photo-nuclear case this is commonly referred to as the vector-meson dominance phenomenon [18]). It seems obvious now that hadron-like processes, such as the ion–ion collision discussed here, behave at intermediate energies, like weakly interacting systems owing to the diminishing value, at these energies, of the total nucleon–nucleon cross section, the basic microscopic quantity for these systems. In the next section we investigate, within more realistic calculations, the behaviour of σ_R and T as a function of the combined radius of the heavy-ion system.

So far we have discussed the total reaction cross section within a one-channel (optical) description of the elastic scattering process. In many instances, a more general description of nuclear absorption, based on the coupled-channels theory, is called for. Thus, in the following we present such a description for the purpose of completeness and in order to develop a theoretical framework through which improvements upon the multiple scattering calculation, presented in the bulk of this paper, can be eventually made.

We introduce now the projection operators, P_0, P' and Q, which project out, respectively, the elastic channel, the directly coupled nonelastic channels and the closed channels (fusion). The elimination of the Q-subspace and the energy average performed subsequently, results in an effective $P_0 + P' = P$ coupled channels. The aim now is to evaluate the total reaction cross section in P_0.

The equation for the elastic element of the T-matrix becomes now, instead of eq. (2.1),

$$P_0TP_0 = P_0VP_0 + P_0VPG_0^{(+)}PTP_0\,, \tag{2.33}$$

which may also be written in the following equivalent form:

$$P_0TP_0 = U_{\rm opt} + U_{\rm opt}P_0G_0^{(+)}P_0TP_0\,, \tag{2.34}$$

$$U_{\rm opt} = P_0VP_0 + P_0VP'G^{(+)}P'VP_0\,, \tag{2.35}$$

where $P'G^{(+)}P'$ is the effective, exact propagator in the P'-subspace.

Of course the discussion presented earlier following eq. (2.1) can be immediately applied to eq. (2.34), with the only difference that the structure of the effective optical potential operator $U_{\rm opt}$ is now fully exhibited in eq. (2.35). Using eq. (2.35) in (2.5), which we write now as

$$\begin{aligned} P_0(T-T^\dagger)P_0 = {} & P_0\Omega^{(+)\dagger}P_0(U_{\rm opt}-U_{\rm opt}^\dagger)P_0\Omega^{(+)}P_0 \\ & -2\pi{\rm i}P_0T^\dagger P_0\delta(E-H_0)P_0TP_0\,, \end{aligned} \tag{2.36}$$

we have

$$\begin{aligned} P_0(T-T^\dagger)P_0 = {} & P_0\Omega^{(+)\dagger}P(V-V^\dagger)P_0\Omega^{(+)}P_0 \\ & + P_0\Omega^{(+)\dagger}P_0[P_0VP'G^{(+)}P'VP_0-(P_0VP'G^{(+)}P'VP_0)^\dagger]P_0\Omega^{(+)}P_0 \\ & -2\pi{\rm i}P_0T^\dagger P_0\delta(E-H_0)P_0TP_0\,. \end{aligned} \tag{2.37}$$

Note that $V\neq V^\dagger$ owing to the averaged out closed channels (fusion).

Assuming now that the P_0P coupling interaction is Hermitian $V_{PP_0}=(V_{P_0P})^\dagger$, which is a reasonable approximation if we consider that the effect of the averaged out Q-space results mostly in an imaginary contribution to the diagonal terms, $U_{P_0P_0}$ and U_{PP} [which appears in (2.34)], we have the following for the second term on the RHS of eq. (2.37):

$$\begin{aligned} & P_0\Omega^{(+)\dagger}P_0VP'(P'G^{(+)}P'-P'G^{(+)\dagger}P')PVP_0\Omega^{(+)}P_0 = P_0\Omega^{(+)\dagger}P_0VP' \\ & \times\left(-2\pi{\rm i}\sum_{P'}|\psi_{P'}^{(-)}\rangle\langle\psi_{P'}^{(-)}| + P'G^{(+)\dagger}P'(V-V^\dagger)G^{(+)}P'\right)P'VP_0\Omega^{(+)}P_0\,. \end{aligned} \tag{2.38}$$

The above result is a consequence of an identity satisfied by the Green function $P'G^{(+)}P'$. Using the fact that the Möller operator P' defining the channels is

$$P'\Omega^{(+)}P_0 = P'G^{(+)}P'VP_0\Omega^{(+)}P_0\,, \tag{2.39}$$

we can now write for $P_0(T-T^\dagger)P_0$, eq. (2.36), the following expression:

$$P_0(T-T^\dagger)P_0 = P_0\Omega^{(+)\dagger}P_0(V-V^\dagger)P_0\Omega^{(+)}P_0 + P_0\Omega^{(+)\dagger}P'(V-V^\dagger)P'\Omega^{(+)}P_0$$
$$-2\pi i\sum_{P'} P_0\Omega^{(+)\dagger}P_0VP'|\psi^{(-)}_{P'}\rangle\delta(E-H_{P_0})\langle\psi^{(-)}_{P'}|P'VP_0\Omega^{(+)}P_0$$
$$-2\pi i P_0T^\dagger P_0\delta(E-H_0)P_0TP_0\,. \tag{2.40}$$

The derivation of the total reaction cross section can now be accomplished using exactly the same steps followed in deriving eq. (2.9). Then

$$\sigma_R = \frac{k}{E_k}\left(\langle\psi^{(+)}_{P_0}|\mathrm{Im}\,V^{(P_0)}|\psi^{(+)}_{P_0}\rangle + \sum_{P'}\langle\psi^{(+)}_{P'}|\mathrm{Im}\,V^{P'}|\psi^{(+)}_{P'}\rangle\right) + \sigma_D\,, \tag{2.41}$$

where σ_D represents the direct reaction contribution to σ_R and it corresponds to the third term on the rhs of eq. (2.40). The first term in the above equation represents absorption in the P_0 and P' channels owing to coupling to the closed-channel subspace, and thus it corresponds to fusion. The above general expression for the fusion cross section has recently been used in discussing heavy-ion fusion at low energies where coupled-channels effects seem to be important [19–21].

Clearly eq. (2.41) is, in principle, equivalent to eq. (2.9), as long as the optical potential used in the latter represents the exact interaction in the elastic channel. The decomposition of σ_R into the distinct terms, namely σ_F and σ_D is, however, quite useful in discussing the reactive content of microscopically derived optical potentials. The $t\rho_1\rho_2$ interaction analysed fully in the following chapters represents but one term in σ_D. This may well be the dominant term at intermediate and high energies. However, at lower energies, we expect that σ_F and the other terms in σ_D such as inelastic channels, to be by far the dominant terms in σ_R. The derivation of the above result using the Wronskian is presented in appendix A.

To end this chapter, we comment briefly on the possible need of using a relativistic description of heavy-ion elastic scattering especially at $E_{CM}/A > 200$ MeV/nucleon, where recent research in proton–nucleus scattering seems to indicate the starting point in such a description in the optical Dirac equation with combined scalar and time-component vector potentials employed as an interaction [22].

Our aim is to assess the importance of the relativistic effects on σ_R. For the purpose we have evaluated σ_R for proton scattering on ^{40}Ca and ^{208}Pb [23]. The details of this calculation are presented fully in section 5. Our results indicate very little difference between the relativistic and nonrelativistic σ_R. We therefore reach the conclusion that a nonrelativistic calculation of σ_R for heavy ions at energies up to $E_{CM}/A = 800$ MeV/nucleon, should be quite adequate. In section 3 we discuss in detail the nonrelativistic $t\rho_1\rho_2$ interaction.

3. Multiple-scattering theory

3.1. Proton–nucleus $t\rho$ interaction

In this subsection we discuss in detail the microscopic nucleon–nucleus optical potential. We do this for two reasons. The first one is that this interaction has been the subject of intensive theoretical investigation for more than 25 years, which resulted in quite a satisfactory status, and the second being that, in principle, the nucleus–nucleus optical potential can be defined in terms of the nucleon–nucleus

interaction through a folding integral (single folding). Of particular interest is the discussion of the reactive content of the nucleus–nucleus interaction, given the structure of the underlying nucleon–nucleus optical potential. This is important for a better understanding of the nature of the total HI reaction cross section at intermediate energies, which has received great attention recently.

A simple, first trial, guess at the form of the nucleon–nucleus potential is the classical relation

$$U(\boldsymbol{r}) = \int \mathrm{d}\boldsymbol{r}'\ \rho(\boldsymbol{r}')V(\boldsymbol{r}, \boldsymbol{r}')\,,$$

where $V(\boldsymbol{r}', \boldsymbol{r})$ is a properly antisymmetrized projectile-nucleon–target-nucleon interaction and $\rho(\boldsymbol{r}')$ is the single-particle (classical) density of the target nucleus (obtained from, e.g., a Hartree–Fock calculation). Clearly the above expression is not entirely correct since, firstly, U is real whereas the optical potential must be complex to account for the nonelastic processes, and secondly, $V(\boldsymbol{r}, \boldsymbol{r}')$ cannot be used as it contains singular components (the "hard core") at $r < 0.4$ fm. What is used instead of $V(\boldsymbol{r}, \boldsymbol{r}')$ is an appropriate effective potential, (or G-matrix) whose hard core is smoothed out, in favor of density dependence [absent from $V(\boldsymbol{r}, \boldsymbol{r}')$].

An apparently different method, usually applied at higher energies is to formulate the problem within a multiple scattering framework. Here one has as an input, the nucleon–nucleon t-matrix (generally off the energy shell). In this paper, we use this latter approach, both in nucleon–nucleus and in nucleus–nucleus scattering. For the purpose of completeness and the presentation of a general frameork, where correction to first-order approximation may be constructed and discussed, we present below the essential ingredients of this approach [24].

The Hamiltonian for the projectile-nucleon–target-nucleus system is written as,

$$H = -(\hbar^2/2m)\nabla^2 + H_{\mathrm{N}} + V\,, \tag{3.1}$$

where H_{N} is the target nucleus Hamiltonian and V is the interaction between the incident nucleon and the target nucleus, which can be written as a sum of individual nucleon–nucleon interactions,

$$V = \sum_{i=1}^{A} V_{\mathrm{p}i}\,. \tag{3.2}$$

The solution of the scattering problem is represented by the full nucleon–nucleus T-matrix

$$T = V + V[E - (H - V) + \mathrm{i}\varepsilon]^{-1}T\,, \tag{3.3}$$

where E is the CM energy. The solution of (3.3) is facilitated by the decomposition

$$T = \sum_i \tau_{\mathrm{p}i}(E)\eta_i(E)\,, \tag{3.4}$$

$$\tau_{\mathrm{p}i} = V_{\mathrm{p}i} + V_{\mathrm{p}i}[E - (H - V) + \mathrm{i}\varepsilon]^{-1}\tau_{\mathrm{p}i}\,. \tag{3.5}$$

Substituting (3.4) into (3.3) gives

$$\eta_i(E) = 1 + \frac{1}{E - (H - V) + \mathrm{i}\varepsilon} \sum_{j \neq i}^{A} \tau_{\mathrm{p}j}(E)\eta_j(E)\,. \tag{3.6}$$

The set of equations (3.4)–(3.6) constitutes the basis of the multiple-scattering series which results in

$$T = \sum_i \tau_{pi}(E) + \sum_{\substack{i \\ j \neq i}} \tau_{pi}(E) \frac{1}{E - (H - V) + i\varepsilon} \tau_{pj}(E) + \cdots . \tag{3.7}$$

At this point it is important to emphasize that the τ_{pi} are not two-body projectile–nucleon transition matrices; the propagator $1/[E - (H - V) + i\varepsilon] \equiv G_0(E)$ contains the *full* nuclear Hamiltonian H_N [see eq. (3.1)] and consequently τ_{pi} is an $(A + 1)$-body operator.

The usual procedure is to replace τ_{pi} by the corresponding nucleon–nucleon T-matrix in free space

$$t_{pi}(E) = \mathcal{V}_{pi} + \mathcal{V}_{pi}(E + \hbar^2\nabla^2/2m + i\varepsilon)^{-1} t_{pi}(E) . \tag{3.8}$$

The corrections to the replacement $\tau \rightarrow t$ resides in corrections to the free Green function – the replacement of an $(A + 1)$-body operator by a two-body operator, and to the use of the CM energy of the p + 1 system in the p–N system (which is reasonable if $A^{-1} \ll 1$).

The stage is now set for obtaining the optical potential operator which is formally defined by the equation

$$T = \mathcal{V} + \mathcal{V}[P_0(E + \hbar^2\nabla^2/2m - K_A)^{-1}]T , \tag{3.9}$$

where $P_0 \equiv |\Psi_0\rangle\langle\Psi_0|$, is the projection operator onto the target-nucleus ground state, and K_A represents the kinetic energy of the CM of the nucleus. Then

$$\begin{aligned} \mathcal{V} &= T(E) - T(E)G_0(E)T(E) + \cdots \\ &= \sum_i^A t_i(E) + \sum_{i \neq j}^A t_i(E) \frac{1 - P_0}{E + (\hbar^2/2m)\nabla^2 - K_A} t_j(E) + \cdots . \end{aligned} \tag{3.10}$$

The ground state matrix element of $\mathcal{V}$ gives us the optical potential for elastic scattering, via

$$\mathcal{V}(E) = \langle \boldsymbol{k}, \boldsymbol{n}', 0 | \mathcal{V} | \boldsymbol{k}, 0, 0 \rangle = (2\pi)^3 \delta(\boldsymbol{k}' + \boldsymbol{n}' - \boldsymbol{k}) \mathcal{V}(\boldsymbol{k}', \boldsymbol{k}, E) , \tag{3.11}$$

where $\boldsymbol{n}'$ is the center-of-mass momentum of the target nucleus, and $\boldsymbol{k}$ is the momentum of the projectile. The first-order potential obtained from eq. (3.10) reads

$$\mathcal{V}^{(1)}(\boldsymbol{k}', \boldsymbol{k}; E) = \int \frac{d\boldsymbol{p}_1}{(2\pi)^3} \phi_0(\boldsymbol{p}_1 + \boldsymbol{q}; \boldsymbol{p}_1) t(\boldsymbol{k}_1', \boldsymbol{k}_1; E') , \tag{3.12}$$

where ϕ_0 is the target-nucleus density matrix, which is related to the density by

$$\begin{aligned} &\rho(\boldsymbol{q}) = \int \frac{d\boldsymbol{p}_1}{(2\pi)^3} \phi_0(\boldsymbol{p}_1 + \boldsymbol{q}; \boldsymbol{p}_1) , \\ &\boldsymbol{q} = \boldsymbol{k}' - \boldsymbol{k} , \qquad \boldsymbol{k}_1 = \boldsymbol{k} - (\mu/m)(\boldsymbol{k} + \boldsymbol{p}_1) , \qquad \boldsymbol{k}_1' = \boldsymbol{k}' - (\mu/m)(\boldsymbol{k}' + \boldsymbol{p}_1) , \\ &E' = E - (\boldsymbol{k} + \boldsymbol{p}_1)^2/2(m_p + m) . \end{aligned} \tag{3.13}$$

The next step is to set $\boldsymbol{p}_1 = 0$ in t, which results in the $t\rho$ expression

$$\mathcal{V}^{(1)}(\boldsymbol{k}', \boldsymbol{k}; E) = \rho(q) t(\boldsymbol{k}_1', \boldsymbol{k}_1; E) \approx \rho(q) t(\theta = 0°; E) . \tag{3.14}$$

The last form ignores off-shell effects. It has the advantage of supplying a model-independent procedure for discussing nucleon–nucleus elastic scattering. The reactive content of $\mathcal{V}^{(1)}$, as is known, is quasifree knock-out [13]. It is to be expected that the impulse-approximation form of $\mathcal{V}^{(1)}$, eq. (3.14) would be valid at intermediate proton energies ($E_p \sim 100$ MeV). At these energies, the nucleon–nucleon scattering is practically purely elastic (except for a very small bremsstrahlung emission). At higher energies, pion production becomes important ($E_{pN}^{CM} \simeq 140$ MeV). This is clearly seen from fig. 1, showing the total reaction cross section for the free nucleon–nucleon system. Clearly medium effects modify this picture to some extent (e.g., shifting the pion production threshold to lower energies). Further, these same nuclear medium effects [5] like Pauli blocking and Fermi motion of the target nucleus, bring about changes in the form of $\mathcal{V}^{(1)}$ (validity of impulse approximation) as well as make higher-order corrections, related to nucleon–nucleon correlations, more important.

Among the numerous corrections required for a better treatment of the scattering process, the second-order double-scattering effect seems to be the easiest to estimate. In momentum space (using the free nucleon–nucleon t-matrix as basic input) [25] this term looks like

$$\langle \boldsymbol{k}', 0|\mathcal{V}^{(2)}|\boldsymbol{k}, 0\rangle = \sum_{i=1}^{A} \sum_{j\neq i} \sum_{\alpha} \int \frac{\mathrm{d}\boldsymbol{k}''}{(2\pi)^3} \langle \boldsymbol{k}', 0|t_i|\boldsymbol{k}'', \alpha\rangle (E - \hbar^2 k''^2/2m - E_\alpha + \mathrm{i}\varepsilon)^{-1} \langle \boldsymbol{k}'', \alpha|t_j|\boldsymbol{k}, 0\rangle . \tag{3.15}$$

Several approximations are usually employed to simplify the above equation. We use an average nuclear excitation energy in the free Green function, $E_\alpha \to \bar{E}_\alpha \equiv \bar{E}$, employ closure to get rid of the $\Sigma_{\alpha\neq 0} \equiv \Sigma_\alpha - |0\rangle\langle 0|$, and employ the eikonal (high-energy approximation) in evaluating the Green's function. Introducing the two-particle correlation function

$$P^{(2)}(\boldsymbol{r}', \boldsymbol{r}) = \frac{1}{A(A-1)} \int \psi_0^+(\boldsymbol{r}_1, \ldots, \boldsymbol{r}_A) \sum_{i=1}^{A} \sum_{j\neq i} \delta(\boldsymbol{r}' - \boldsymbol{r}_i)\delta(\boldsymbol{r} - \boldsymbol{r}_j)\psi_0(\boldsymbol{r}_1, \ldots, \boldsymbol{r}_A)\, \mathrm{d}\boldsymbol{r}_1 \cdots \mathrm{d}\boldsymbol{r}_A , \tag{3.16}$$

one can then write an approximate form for the double scattering contribution. In coordinate space it looks like

$$\mathcal{V}^{(2)}(r) \simeq -(\mathrm{i}k/2E)[\mathcal{V}^{(1)}(r)]^2 R_{\mathrm{corr}} , \tag{3.17}$$

where $\mathcal{V}^{(1)}$ is the first-order $t\rho$ potential and R_{corr} is the two-particle correlation length, given by

$$R_{\mathrm{corr}} = \int_0^\infty \left(\frac{P^{(2)}(\boldsymbol{r}', \boldsymbol{r})}{\rho(r')\rho(r)} - 1 \right)_{(|\boldsymbol{r}-\boldsymbol{r}'|)} \mathrm{d}(\boldsymbol{r} - \boldsymbol{r}') . \tag{3.18}$$

Here a further assumption on the quantity $P^{(2)}/\rho\rho$ has been made, namely that it depends only on the relative separation between the two nucleons and not on their individual positions. In the absence of two-body correlations, $R_{\mathrm{corr}} = 0$. In general, it is expected that $P^{(2)}(\boldsymbol{r}', \boldsymbol{r})$ would approach the no-

correlation form at a separation larger than the hard core radius (~0.4 fm). At smaller separations $P^{(2)} = 0$. Thus $R_{\rm corr} \cong -0.4$ fm.

The estimate given above for $R_{\rm corr}$ is very crude. In a more refined treatment of $R_{\rm corr}$ presented by Ray [26] it is actually composed of four distinct contributions,

$$R_{\rm corr} = R_{\rm Pauli} + R_{\rm SRD} + R_{\rm PSR} + R_{\rm CM} \,. \tag{3.19}$$

Following Boridy and Feshbach [27], $R_{\rm Pauli}$ is related to the Pauli exclusion-principle correlations, $R_{\rm SRD}$ is related to the short-range dynamical correlations and $R_{\rm PSR}$ is connected to the combination of a Pauli and a short-range dynamical term. Finally $R_{\rm CM}$ arises from center-of-mass correlations. We give below the approximate expressions for these four contributions to $R_{\rm corr}$ derived by Ray [26]

$$\begin{aligned}
-R_{\rm Pauli} &= \frac{1}{2}\left(1 - \frac{5}{A} + \frac{4}{A^2}\right) \frac{3\pi}{10\bar{k}_{\rm F}(r)} \frac{1}{1 + \frac{8}{5}\bar{B}k_{\rm F}^2(r)} \,, \\
-R_{\rm SRD} &= \frac{1}{2}\left(1 - \frac{2}{A} + \frac{1}{A^2}\right)\sqrt{\pi}\, \frac{b^3}{b^2 + 8\bar{B}} \,, \\
R_{\rm PSR} &= \frac{1}{2}\left(1 - \frac{5}{A} + \frac{4}{A^2}\right) \frac{3\pi}{10} \left(k_{\rm F}^2(r) + \frac{5}{b^2}\right)^{-1/2} \left[1 + 8\bar{B}\left(\frac{k_{\rm F}^2(r)}{5} + \frac{1}{b^2}\right)\right]^{-1} \,, \\
-R_{\rm CM} &= (1 - 2/A + 1/A^2) l_{\rm c} \,,
\end{aligned} \tag{3.20}$$

where the parameters A, $k_{\rm F}(r)$, $\bar{B}$, b, $l_{\rm c}$ are the target mass number, local Fermi momentum, finite-range parameter of the nucleon–nucleon elastic t-matrix, short-range dynamical correlation parameter and the effective "correlation length", respectively. We should mention that $\bar{B}$ exhibits a non-negligible energy dependence: 0.66 at $E_{\rm LAB} = 100$ MeV and dropping to about 0.1 at $E_{\rm LAB} =$ 2200 MeV.

We have evaluated $R_{\rm corr}$ according to eqs. (3.19) and (3.20) for the system p + ^{12}C at several proton laboratory energies. The results are presented in fig. 5. As can be seen in this figure the dominant contributions to $R_{\rm corr}$ arise from the Pauli and center-of-mass correlations. Further, the values of the calculated $R_{\rm corr}$ over a wide range of proton energies approximates closely the very simple estimate for $R_{\rm corr}$ given earlier, namely −0.411 fm.

We see clearly from our approximate form for $\mathcal{V}^{(2)}$ in eq. (3.17) that the multiple-scattering series is an expansion in terms of the correlation radius. The third- and higher-order terms would depend on three- and many-body correlations. No simple expressions are found for these terms. In the next subsection we shall employ the above theoretical developments for the calculation of the ion–ion interaction at intermediate energies.

3.2. *Nucleus–nucleus $t\rho_1\rho_2$ interaction*

Once the nucleon–nucleus potential operator is constructed, the corresponding nucleus–nucleus potential can in principle, be obtained, with due care for antisymmetrization, by a folding procedure. In discussing heavy-ion reactions at low energies, it has been customary to employ the double folding prescription in conjunction with an effective nucleon–nucleon interaction (G-matrix) which contains most of the nuclear medium effects. A more thorough discussion of this has been given by Satchler and

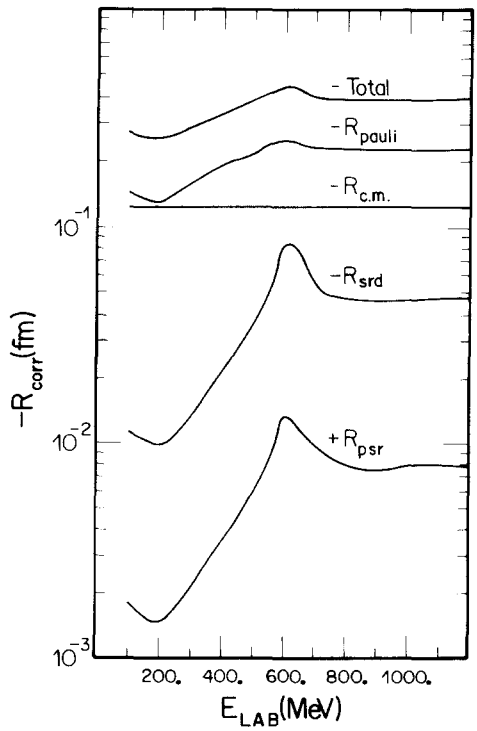

Fig. 5. The correlation distance R_{corr} versus laboratory energy for the p + ^{12}C system. See text for details.

Love [28], who write for the real part of the ion–ion potential

$$\mathrm{Re}\, V = \int \mathrm{d}\boldsymbol{r}_1 \int \mathrm{d}\boldsymbol{r}_2\, \rho_1(\boldsymbol{r}_1)\rho_2(\boldsymbol{r}_2)\mathcal{V}(\boldsymbol{r}_{12} = \boldsymbol{R} + \boldsymbol{r}_2 - \boldsymbol{r}_1)\,, \tag{3.21}$$

where $\mathcal{V}$ is given by the M3y interaction

$$\mathcal{V}(r_{12}) = 6315\,\frac{\mathrm{e}^{-4r_{12}}}{4r_{12}} - 1961\,\frac{\mathrm{e}^{-2.5r_{12}}}{2.5r_{12}} + J_{00}\delta(\boldsymbol{r}_{12})\,, \quad J_{00} = -81\ \mathrm{MeV\,fm}^3\,.$$

The last term in the above expression for $\mathcal{V}$ takes into account the nucleon exchange effects. No energy dependence is present in the above expression. Of course at higher energies, the procedure above should be replaced by the more appropriate nucleon–nucleon G- or t-matrix, which, when inserted in the double folding integral above, would determine the energy dependence of the resulting, *complex* ion–ion potential. Thus, following the discussion of the previous section we write

$$\mathcal{V}^{(1)}_{A_1A_2} \cong t(\theta = 0°; E) \int \mathrm{d}\boldsymbol{r}'\, \rho_{A_1}(\boldsymbol{r})\rho_{A_2}(\boldsymbol{r} - \boldsymbol{r}') = -4\pi\,\frac{E}{k^2}\, f_{\mathrm{NN}}(\theta = 0°; E) \int \mathrm{d}\boldsymbol{r}'_1\, \rho_{A_1}(\boldsymbol{r}')\rho_{A_2}(\boldsymbol{r} - \boldsymbol{r}')\,, \tag{3.22}$$

where f_{NN} is the nucleon–nucleon scattering amplitude. With the help of the optical theorem we may now obtain the imaginary part of $\mathcal{V}^{(1)}_{A_1A_2}(r)$,

$$\text{Im}\, \mathcal{V}^{(1)}_{A_1A_2}(r) = -\frac{E}{k}\,\sigma_{\text{NN}}(E)\int \rho_{A_1}(r')\rho_{A_2}(r-r')\,\mathrm{d}r'\,, \tag{3.23}$$

which is clearly just the proton–nucleus imaginary interaction folded onto the projectile density.

The real part of $\mathcal{V}^{(1)}_{A_1A_2}(r)$, which would correspond to the intermediate energy version of the double folding interaction, can be obtained from the systematics of Re f_{NN}. One usually writes [26]

$$\text{Re}\, f_{\text{NN}} = \alpha\, \text{Im}\, f_{\text{NN}}\,, \qquad \text{Im}\, f_{\text{NN}} = (k\sigma^{\text{T}}_{\text{NN}}/4\pi)\exp(-a_{\text{NN}}q^2)\,. \tag{3.24}$$

The parameter α depends on the nucleon energy, attaining the value of 0.06 at $E_{\text{LAB}} = 800$ MeV and becoming negative at $E > 1000$ MeV. In table 1 we present the values of the physical parameters that determine f_{NN} at several laboratory energies. As a consequence of eq. (3.24) and table 1, the real part of $\mathcal{V}^{(1)}_{A_1A_2}$ at $E/N \simeq 1000$ MeV should become attractive. We turn now to the consideration of the second-order (double-scattering) contribution to the ion–ion potential.

Our recipe for this contribution is to perform a symmetrized single folding with the projectile and target densities. This then suggests

$$\mathcal{V}^{(2)}_{A_1A_2}(r) = -(\mathrm{i}k/4E)R_{\text{corr}}\left(\int [\mathcal{V}_{\text{N}A_1}(r-r')]^2\rho_{A_2}(r')\,\mathrm{d}r' + \int [\mathcal{V}_{\text{N}A_2}(r-r')]^2\rho_{A_1}(r')\,\mathrm{d}r'\right), \tag{3.25}$$

where $\mathcal{V}^{(1)}_{\text{N}A_1}(r)$ is the nucleon–nucleus (A_1) $t\rho$ type optical potential discussed earlier.

We evaluated the second-order (double-scattering) correction to the $t\rho_1\rho_2$ potential, according to eq. (3.25), with R_{corr} given by eqs. (3.19) and (3.20) for the system $^{12}\text{C} + {}^{12}\text{C}$ at the following laboratory energy per nucleon: 100, 200, 300 and 500 MeV. In figs. 6 and 7, we show the radial distribution of the second-order correction to the optical potential for the $^{12}\text{C} + {}^{12}\text{C}$ systems at the above energies. For comparison, we also show the contribution of the dominant $t\rho_1\rho_2$ DF potential at 100 MeV/N. The range of the second-order potential is appreciably shorter than that of the first one owing to the high-order density dependence $(t\rho_1)^2\rho_2$ versus $(t\rho_1)\rho_2$ [29]. It is interesting to note that the imaginary part of the optical potential changes at 100 MeV/N namely, $W^{(2)}$ is regenerative whereas at the other cited energies it is absorptive. We should stress, though, that the sum of the contributions of $W^{(1)}$ and $W^{(2)}$ is guaranteed to be absorptive. The above behaviour of $W^{(2)}$ is a consequence of the folding formula (3.25). Using explicitly the form of $\mathcal{V}^{(1)}$ in eq. (3.20), we have

Table 1
The parameters of the NN amplitude according to eq. (3.24); from ref. [26]

E_{LAB} (MeV)	$\sigma^{\text{T}}_{\text{pp}}$ (mb)	α_{pp}	a_{pp} (fm^2)	$\sigma^{\text{T}}_{\text{pn}}$ (mb)	α_{pn}	a_{pn} (fm^2)
100	33.2	1.87	0.66	72.7	1.00	0.36
150	26.7	1.53	0.57	50.2	0.96	0.58
200	23.6	1.15	0.56	42.0	0.71	0.68
325	24.5	0.45	0.26	36.1	0.16	0.36
425	27.4	0.47	0.21	33.1	0.25	0.27
550	36.9	0.32	0.04	35.5	−0.24	0.085
650	42.3	0.16	0.07	37.7	−0.35	0.09
800	47.3	0.06	0.09	37.9	−0.20	0.12
1000	47.2	−0.09	0.09	39.2	−0.46	0.12
2200	44.7	−0.17	0.12	42.0	−0.50	0.14

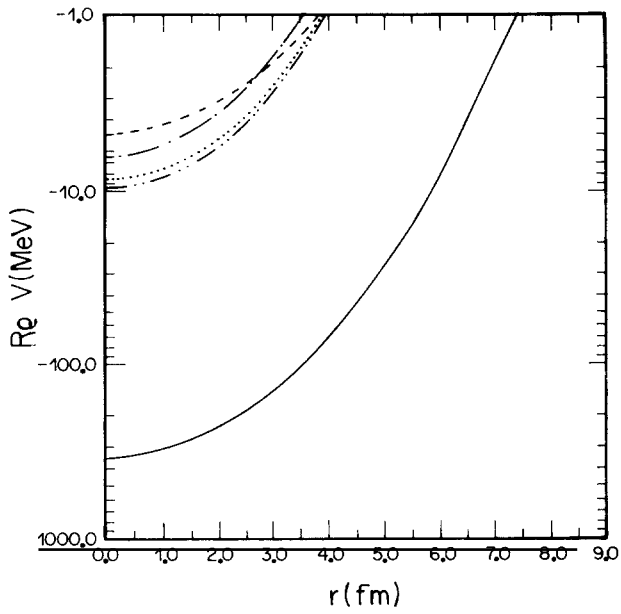

Fig. 6. The real part of the second-order nucleus–nucleus potential at four laboratory energies: 100 MeV/N (dashed curve), 200 MeV/N (dotted curve), 300 MeV/N (dashed–dotted curve) and 500 MeV/N (dashed–double-dotted curve). For reference, the usual double-folding potential is also shown (solid curve).

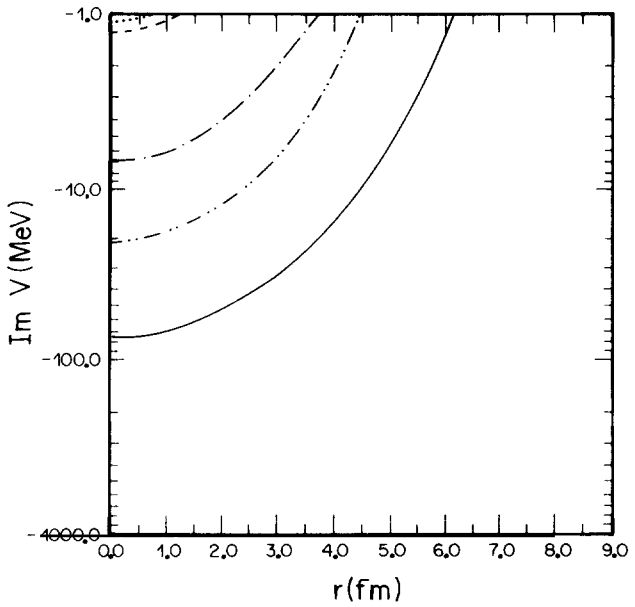

Fig. 7. The imaginary part of the second-order nucleus–nucleus potential (same as fig. 6). The potential equivalent to the double-folding potential, namely Im $t\rho$, ρ_2 is also exhibited (solid curve).

$$\begin{aligned}\text{Re } \mathcal{V}^{(2)} &= -(E/2k)|R_{\text{corr}}|\alpha\sigma_{\text{T}}^2\langle\rho_{A_1}^2\rho_{A_2}+\rho_{A_2}^2\rho_{A_1}\rangle(r)\,,\\ \text{Im } \mathcal{V}^{(2)} &= (E/4k)|R_{\text{corr}}|(\alpha^2-1)\sigma_{\text{T}}^2\langle\rho_{A_1}^2\rho_{A_2}+\rho_{A_2}^2\rho_{A_1}\rangle(r)\,,\end{aligned} \tag{3.26}$$

$$\langle\rho_{A_1}^2\rho_{A_2}+\rho_{A_2}^2\rho_{A_1}\rangle(r)\equiv\int\rho_{A_1}^2(r-r')\rho_{A_2}(r')\,\mathrm{d}r'+\int\rho_{A_2}^2(r-r')\rho_{A_1}(r')\,\mathrm{d}r'\,. \tag{3.27}$$

Therefore Re $\mathcal{V}^{(2)}$, being linear in Re f_{NN} (and correspondingly in the parameter α), is attractive in the energy range 100 MeV $< E <$ 800 MeV and repulsive at $E_{\text{LAB}} >$ 1000 MeV. In contrast Im $\mathcal{V}^{(2)}$ behaves as α^2-1 and thus is regenerative at those energies where $\alpha>1$, and absorptive at the other energies where $\alpha<1$. The sum Im $\mathcal{V}^{(1)}$ + Im $\mathcal{V}^{(2)}$ is guaranteed to be always negative (absorptive) as unitarity requires.

In our calculation of the ion–ion optical potential to be described later, we have used Pauli-blocking corrected nucleon–nucleon total cross sections. The full details of the structure of Im$(\mathcal{V}^{(1)}+\mathcal{V}^{(2)})$, which is used later for the calculation of σ_{R}, are given in the following section. Here we may mention that owing to the fact that the volume integral of $\mathcal{V}^{(2)}$ is 0.3 times that of $\mathcal{V}^{(1)}$, it is expected that the effect of $\mathcal{V}^{(2)}$ on σ_{R} is small. We have verified this by evaluating, within the JWKB approximation discussed in section 2, the total reaction cross section of $^{12}\text{C}+{}^{12}\text{C}$ using $\mathcal{V}^{(1)}+\mathcal{V}^{(2)}$ for an optical potential and have found that $\mathcal{V}^{(2)}$ has an influence of less than 10% on σ_{R}, as compared with the calculation with only $\mathcal{V}^{(1)}$ included. In our calculation, to be described fully in section 4, we have included the Pauli-blocking effect mentioned above, and performed an appropriate average over the Fermi motion of the nucleon in the projectile and target.

4. The imaginary part of the $t\rho_1\rho_2$ interaction

In this section we develop further the theory of the imaginary part of the ion–ion potential discussed in the previous section. In particular we investigate the effect of Pauli blocking on the potential and the subsequent effect on the mean free path. Other medium effects such as the binding energy, off-shell effects and the non-locality of the potential will also be briefly discussed.

As we saw in the previous section, the imaginary part of the $t\rho_A\rho_B$ interaction, can be written in the following form:

$$W(E;\boldsymbol{r})=-\frac{E}{k_N}\,\sigma_{\text{T}}^{\text{NN}}(E)\int\mathrm{d}\boldsymbol{r}'\rho_A(\boldsymbol{r}-\boldsymbol{r}')\rho_B(\boldsymbol{r}')\,, \tag{4.1}$$

where E and k_{N} are the energy and momentum per nucleon, respectively, and $\sigma_{\text{T}}^{\text{NN}}$ is the nucleon–nucleon total cross section. The Pauli blocking is included in the above expression for W, by modifying (reducing) $\sigma_{\text{T}}^{\text{NN}}$. According to Kikuchi and Kawai [30] this entails substituting $\sigma_{\text{T}}^{\text{NN}}$ above by an average cross section given (for the case of proton–nucleus scattering) by

$$\bar{\sigma}_{\text{T}}^{\text{NN}}(E)=\frac{1}{k_1(\frac{4}{3}\pi k_{\text{F}}^3)}\int\mathrm{d}\boldsymbol{k}_2\int\mathrm{d}\Omega'\,2k\sigma_{\text{NN}}(\boldsymbol{k},\boldsymbol{k}')\,, \tag{4.2}$$

where it is assumed that $\boldsymbol{k}_1$ is the momentum of the projectile nucleon, k_{F} is the Fermi momentum of the target, $\boldsymbol{k}_2$ is the momentum of a target nucleon, $\mathrm{d}\Omega'$ is the element of solid angle that defines the

direction of the final relative momentum $\boldsymbol{k}'$; $\boldsymbol{k}$ is the initial relative momentum and $\sigma_{\rm NN}(\boldsymbol{k},\boldsymbol{k}')$ is the differential NN cross section. The integrals appearing in eq. (4.2) take into account the Pauli blocking through the restriction imposed on $|k_2|<k_{\rm F}$ and on $\mathrm{d}\Omega'$. Assuming an isotropic angular distribution of $\sigma(\boldsymbol{k},\boldsymbol{k}')=(1/4\pi)\sigma_{\rm T}^{\rm NN}(k)$, one is then able to derive for $\bar{\sigma}_{\rm T}^{\rm NN}$, the following simple expression [31]:

$$\bar{\sigma}_{\rm T}^{\rm NN}(E)=\sigma_{\rm T}^{\rm NN}(E)P(E_{\rm F}/E)\,, \tag{4.3}$$

$$P(X)=\begin{cases}1-\frac{7}{5}X\,, & X\le\frac{1}{2}\,,\\ 1-\frac{7}{5}X+\frac{2}{5}X(2-X^{-1})^{5/2}\,, & X\ge\frac{1}{2}\,.\end{cases} \tag{4.4}$$

In obtaining eq. (4.3), it is assumed that the free nucleon–nucleon total cross section is independent of energy, which is a reasonable assumption at energies above 100 MeV. Assuming that the cross section is inversely proportional to the energy, $P(X)$ attains the form $P(X)=1-\frac{8}{5}X$.

For the nucleus–nucleus interaction, eq. (4.1), the Pauli blocking effect is incorporated into $\bar{\sigma}_{\rm T}^{\rm NN}$ since both projectile and target nucleons are Pauli blocked. No simple expression for $P(X)$ is obtained in this case and only through numerical integrations is one able to obtain $\bar{\sigma}_{\rm T}^{\rm NN}$. Nonetheless, analytical formulas are obtainable for the allowed scattering solid angle [60]. The pertinent formulae as well as the details of the calculation are given in appendix C.

The above Pauli blocking is taken into consideration in nuclear matter. In actual finite nuclei we invoke two straightforward modifications on the results obtained so far: firstly, the local density approximation, which renders $k_{\rm F}$ dependent on the radial distance, through $k_{\rm F}(\rho(r))$,

$$k_{\rm F}=[\tfrac{3}{2}\pi^2\rho(r)]^{1/3}\,, \tag{4.5}$$

and secondly, we use an average nucleon–nucleon cross section. For nucleon–nucleus scattering we have

$$\langle\bar{\sigma}_{\rm T}^{\rm NN}\rangle=[(A-Z)\bar{\sigma}_{\rm Nn}+Z\bar{\sigma}_{\rm Np}]/A\,, \tag{4.6}$$

where N refers to n or p according to whether the incident nucleon is proton or neutron, respectively. In the absence of Pauli blocking, one expects from eq. (4.6) that generally $\langle\bar{\sigma}_{\rm T}^{\rm pN}\rangle$ is larger than the free p–p or n–n cross section. Of course for $N=Z$ nuclei,

$$\langle\bar{\sigma}_{\rm T}^{\rm NN}\rangle=\tfrac{1}{2}(\bar{\sigma}_{\rm T}^{\rm Nn}+\bar{\sigma}_{\rm T}^{\rm Np})=\tfrac{1}{2}(\sigma_{\rm T}^{\rm Nn}+\sigma_{\rm T}^{\rm Np})P(E_{\rm F}/E)\,. \tag{4.7}$$

The symmetrized $\bar{\sigma}_{\rm T}^{\rm NN}$ relevant for nucleon–nucleus scattering has the form

$$\langle\bar{\sigma}_{\rm T}^{\rm NN}\rangle=\frac{Z_1Z_2+(A_1-Z_1)(A_2-Z_2)}{A_1A_2}\,\bar{\sigma}_{\rm T}^{\rm Nn}+\frac{Z_1(A_2-Z_2)+Z_2(A_1-Z_1)}{A_1A_2}\,\bar{\sigma}_{\rm T}^{\rm Np}\,.$$

Since within the local-density approximation $\bar{\sigma}_{\rm T}^{\rm NN}$ and $\langle\bar{\sigma}_{\rm T}^{\rm NN}\rangle$ are r-dependent, the expression for W in eq. (4.1), becomes

$$W(E;r)=-\frac{E}{k_{\rm N}}\int \mathrm{d}\boldsymbol{r}'\;\rho_A(\boldsymbol{r}-\boldsymbol{r}')\rho_B(\boldsymbol{r}')\langle\bar{\sigma}_{\rm T}^{\rm NN}\rangle[E,k_{\rm F}^A(r,r');k_{\rm F}^B(r')]\,. \tag{4.8}$$

To take better account of the surface, we have also corrected $k_{\rm F}(r)$ [32],

$$[k_F^i(r)]^2 = [\tfrac{3}{2}\pi^2\rho_i(r)]^{2/3} + \tfrac{5}{2}(\nabla\rho_i/\rho_i)^2\xi\ , \tag{4.9}$$

where ξ is of the order of 0.1. The above form of k_F is the one employed in the calculation of W in eq. (4.8). The Fermi momentum of each nucleus has been determined using eq. (4.9) by dividing the space occupied by the nucleus into three regions, internal, central and surface.

Using the above as well as the results of appendix D we have calculated the Pauli-blocking modified NN cross sections. In figs. 8 and 9 we present the behaviour of σ_{pp} and σ_{np} versus k. Also shown are the free-space cross sections. Different values of the Fermi momentum of the target nucleus, k_{F1}, k_{F2}, were used for the purpose of comparison. In figs. 10 and 11 are shown the effective σ_{NN} appropriate for nucleus–nucleus scattering, for different values of the Fermi momenta k_{F1} and k_{F2} of the two ions.

From these figures, one can see clearly that the Pauli-blocking reduction in the values of σ_{NN} is greater in the nucleus–nucleus systems than in the nucleon–nucleus systems at higher energies. At lower energies the situation is reversed quite drastically. In fact at $k < k_F$, the nucleon–nucleon cross sections in the nucleon–nucleus case approach zero. On the other hand, at these low energies the nucleus–nucleus σ_{np} and σ_{pp} is non-negligible. This is so due to the increased role of the surface

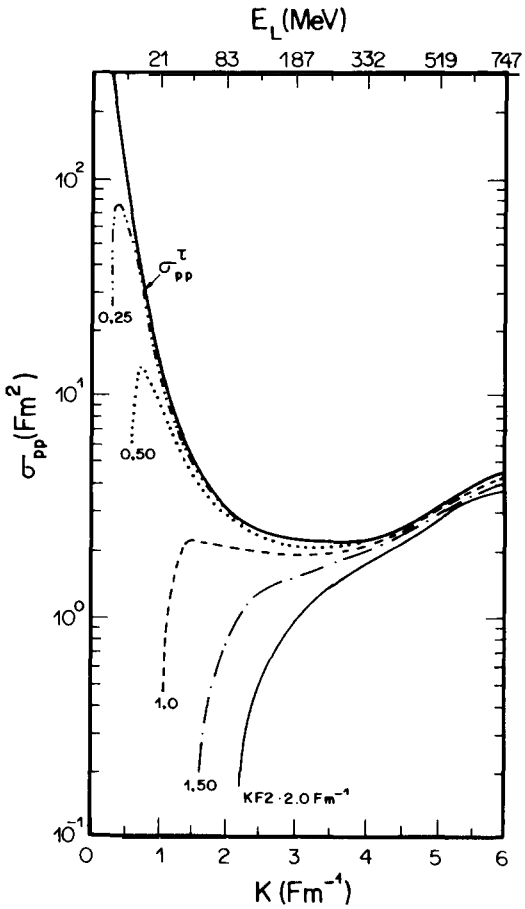

Fig. 8. The Pauli blocking-corrected total proton–proton cross section in the proton–nucleus system, for several values of k_{F2} (the target Fermi momentum). Also shown is the free σ_T^{pp}.

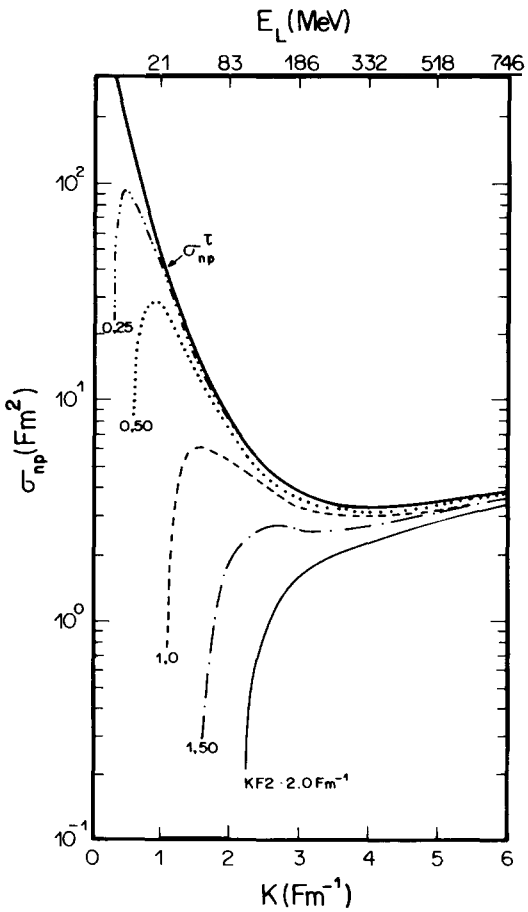

Fig. 9. Same as fig. 8 for the neutron–proton total cross section in the proton–nucleus system.

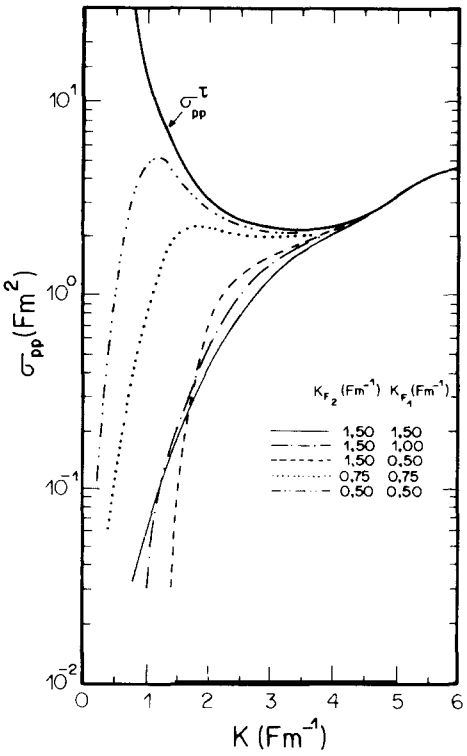

Fig. 10. Same as fig. 8 in the nucleus–nucleus system.

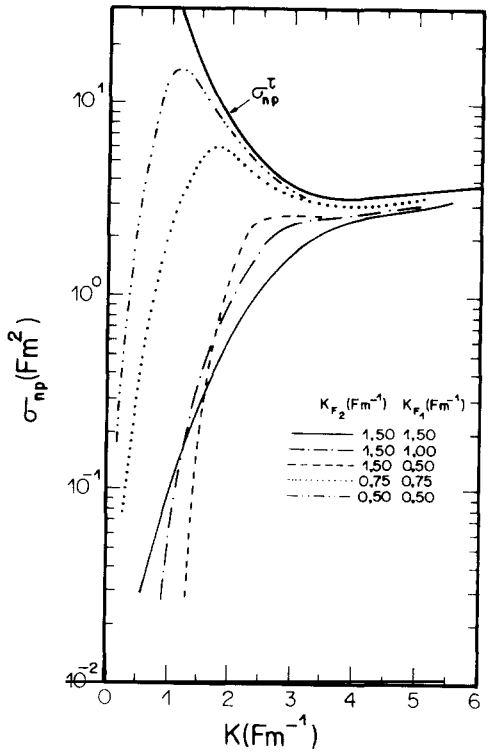

Fig. 11. Same as fig. 9 in the nucleus–nucleus system.

nucleons that still have enough energy owing to Fermi motion which enables them to scatter nucleons into the Pauli allowed angular region.

It is commonly assumed that the total nucleon–nucleon cross section in free space is a slowly varying function of energy and is consequently replaced by a constant. Such a procedure is used, e.g., to derive the Pauli-modified cross section, eq. (4.3). However, in the energy region of interest to us, the energy dependence of the free cross sections is quite strong and has to be taken into account, as we have done here.

We are now in a position to calculate W. In figs. 12 and 13 we present our results for two systems. Also shown is the W evaluated with the free σ_T^{NN}, for comparison. Clearly Pauli blocking reduces greatly the strength of W at lower energies as expected. At intermediate and high energies the Pauli-blocking effect is reduced in importance, and W approaches the value with free σ_T^{NN}. We should mention that at low energies, other reaction mechanisms besides single-nucleon knockout come into play rendering our calculated W with Pauli blocking certainly smaller than the W extracted from adjustment of the total reaction cross section. This we discuss fully in the following sections. To take into account the effect of these other mechanisms, one has to have a model for W which accounts for collective surface excitation, as well as for fusion.

Before proceeding with a calculation of σ_R for several systems, it is relevant to assess the importance of another effect, which is completely alien to the formalism developed so far, namely relativity. By relativity, we mean the actual relativistic treatment of the particles involved and the use of the Dirac equation. Therefore, we dedicate the next section to this question and consider specifically p–nucleus scattering.

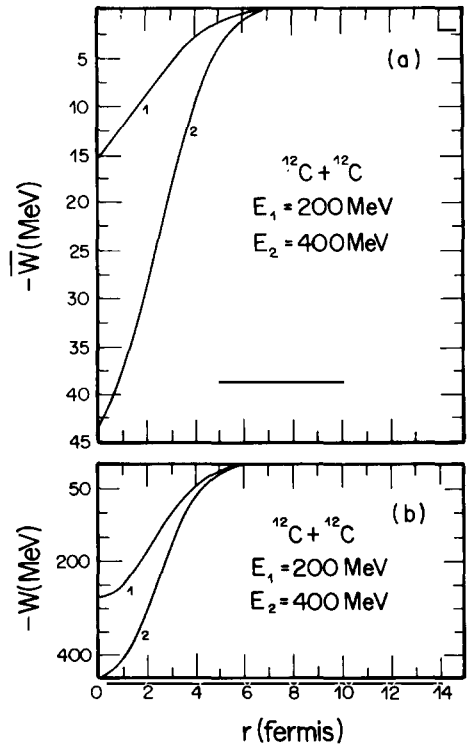

Fig. 12. The imaginary part of the $t\rho_1\rho_2$ interaction for $^{12}C + ^{12}C$: (a) with Pauli blocking; (b) without Pauli blocking.

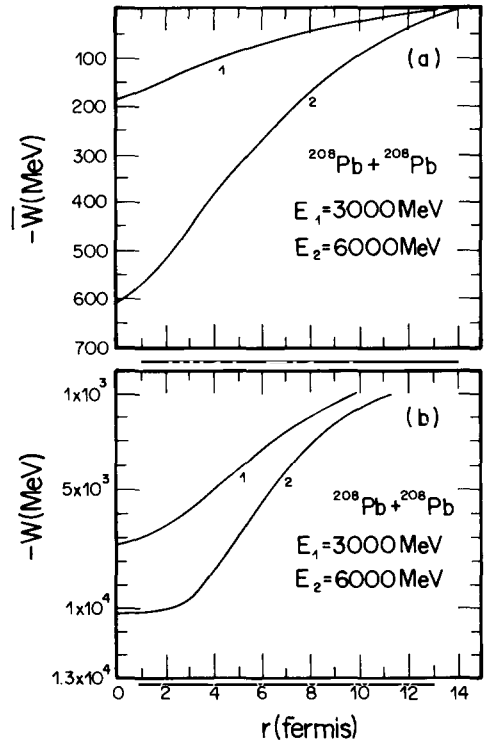

Fig. 13. Same as fig. 12 for the $^{208}Pb + ^{208}Pb$ system.

5. Relativistic Dirac form of the total reaction cross section

The discussion and calculation of σ_R presented in this paper was based on nonrelativistic scattering theory. In recent years, it has become quite clear that proton–nucleus scattering at intermediate energies is more correctly described by a relativistic Dirac optical equation. In particular, spin polarization and rotation seem quite clearly to require, for their description, such a relativistic theory [33, 34]. One would also like to check whether such a relativistic theory will influence σ_R. In this section, we present the relativistic formulation of σ_R and apply it to proton–nucleus scattering [23].

The Dirac equation that describes the elastic scattering of a nucleon, treated as a Dirac particle, from a spin-saturated nucleus, is usually formulated using a time-dependent description,

$$[\boldsymbol{\alpha}\cdot\boldsymbol{p} + \beta(m + V_s) + V_0]\psi = E\psi\,, \tag{5.1}$$

where it is assumed that the average, complex, nucleon–nucleus potential is a sum of a scalar component, V_s and the fourth (time) component of a vector potential, V_0. The matrices $\boldsymbol{\alpha}$ and β are Dirac's, and ψ is the four-component vector wavefunction.

Let us write V_s and V_0 as

$$V_s = U_s - iW_s\,, \qquad V_0 = U_0 - iW_0\,. \tag{5.2}$$

Equation (5.2) can be rewritten as

$$[\gamma_4(E - V_0) - \mathrm{i}\boldsymbol{\gamma}\cdot\boldsymbol{p} - (m + V_s)]\psi = 0\,, \tag{5.3}$$

obtained from the usual relations, $\mathrm{i}\boldsymbol{\gamma} \equiv \gamma_4\boldsymbol{\alpha}$, $\gamma_4 \equiv \beta$. We now perform the usual manipulations of multiplying eq. (5.3) from the left by $\bar{\psi} = \psi^\dagger\gamma_4$ and constructing its conjugate with the subsequent multiplication from the right by ψ, to obtain finally

$$\bar{\psi}[\gamma_4(E - V_0) - \mathrm{i}\boldsymbol{\gamma}\cdot\boldsymbol{p} - (m + V_s)]\psi = 0\,, \tag{5.4}$$

$$\bar{\psi}[\gamma_4(E - V_0^\dagger) - \mathrm{i}\boldsymbol{\gamma}\cdot\boldsymbol{p} - (m + V_s^\dagger)]\psi = 0\,. \tag{5.5}$$

The usual Wronskian argument used in appendix A now supplies us with the continuity equation

$$-\boldsymbol{\nabla}\cdot\boldsymbol{j} = (2/\hbar)(\psi^\dagger W_0\psi + \psi^\dagger\gamma_4 W_s\psi)\,. \tag{5.6}$$

The hadronic current is

$$\boldsymbol{j} = \mathrm{i}\bar{\psi}\boldsymbol{\gamma}\psi\,. \tag{5.7}$$

Integrating eq. (5.6) over a large volume and using Gauss' theorem, gives us

$$-\int_S \boldsymbol{j}\cdot\mathrm{d}\boldsymbol{A} = \frac{2}{\hbar}\,\langle\psi^{(+)}|W_0 + \gamma_4 W_s|\psi^{(+)}\rangle\,, \tag{5.8}$$

where the integral is over a surface surrounding the potential, in a region where the potential has completely vanished, and describes the net inward flux due to absorption ($W_0 \neq 0$, $W_s \neq 0$). Dividing this flux by the incident current $v/[1 - (v/c)^2]^{1/2} \equiv v\gamma$ (assuming that $\psi^{(+)}$ is normalized to unity), gives the total reaction cross section

$$\sigma_R = -\Big(\int_{S\to\infty} \boldsymbol{j}\cdot\mathrm{d}\boldsymbol{A}\Big)(v\gamma)^{-1} = \frac{2}{\hbar v\gamma}\,\langle\psi^{(+)}|W_0 + \gamma_4 W_s|\psi^{(+)}\rangle\,. \tag{5.9}$$

We remind the reader again that $\psi^{(+)}$ is a scattering vector wavefunction.

Equation (5.9) can be further reduced to a form more convenient for numerical evaluation. We do this by explicitly writing $\psi^{(+)}$ in terms of its upper (large) and lower (small) components,

$$\psi^{(+)} = \left(\frac{E + m}{2m}\right)^{1/2}\begin{pmatrix} 1 \\ (1/A)\boldsymbol{\sigma}\cdot\boldsymbol{p}\end{pmatrix}u_s\,, \tag{5.10}$$

where $A = E + m + V_s - V_0$, and u_s satisfies the reduced Dirac equation

$$[(\boldsymbol{\sigma}\cdot\boldsymbol{p})A^{-1}(\boldsymbol{\sigma}\cdot\boldsymbol{p}) - E - m - V_s - V_0]u_s = 0\,. \tag{5.11}$$

With eq. (5.10) σ_R of eq. (5.9) becomes

$$\sigma_{\mathrm{R}} = \frac{E+m}{\hbar v \gamma m}\left\{\int \mathrm{d}^3 r\left[(W_0+W_{\mathrm{s}})u_{\mathrm{s}}^{\dagger}u_{\mathrm{s}} - (W_{\mathrm{s}}-W_0)\left(\frac{1}{A}\,\boldsymbol{\sigma}\cdot\boldsymbol{p}u_{\mathrm{s}}\right)^{\dagger}\left(\frac{1}{A}\,\boldsymbol{\sigma}\cdot\boldsymbol{p}u_{\mathrm{s}}\right)\right]\right\}. \tag{5.12}$$

Using the fact that $(W_{\mathrm{s}}-W_0)/|A|^2 = (A^{-1}-A^{\dagger -1})/2\mathrm{i}$, we can, after performing one integration by parts and using Gauss' theorem on the second term on the rhs of eq. (5.12), write for σ_{R} the following surface integral:

$$\sigma_{\mathrm{R}} = -\frac{1+\gamma}{2v\gamma}\int_s \mathrm{d}A\left[u_{\mathrm{s}}^{\dagger}\left(\frac{\boldsymbol{\sigma}\cdot\hat{\boldsymbol{n}}}{A}\,\boldsymbol{\sigma}\cdot\boldsymbol{p}u_{\mathrm{s}}\right) + \left(\frac{\boldsymbol{\sigma}\cdot\hat{\boldsymbol{n}}}{A}\,\boldsymbol{\sigma}\cdot\boldsymbol{p}\right)^{\dagger}u_{\mathrm{s}}\right], \tag{5.13}$$

which reduces, in the appropriate limit $s\to\infty$, where $A\to E+m=(1+\gamma)m$, to the final expression

$$\sigma_{\mathrm{R}} = -\frac{1}{mv\gamma}\int_{s\to\infty}\mathrm{d}A\,\mathrm{Re}(u_{\mathrm{s}}^{\dagger}\boldsymbol{\sigma}\cdot\hat{\boldsymbol{n}}\boldsymbol{\sigma}\cdot\boldsymbol{p}u_{\mathrm{s}}). \tag{5.14}$$

Equation (5.14) could have been obtained directly from the first part of eq. (5.9) namely from the identification $\sigma_{\mathrm{R}} = -(\int_{s\to\infty}\mathrm{d}\boldsymbol{A}\cdot\boldsymbol{j})/\gamma v$. Our derivation above serves as a check of the correctness of eq. (5.9). In the following, we evaluate eq. (5.14) in the eikonal (small-angle) limit.

The eikonal approximation to $\psi^{(+)}$ or u_{s} of eq. (5.1) or eq. (5.11), has been recently discussed by Amado et al. [35]. Here we derive an eikonal form from σ_{R}, starting with eq. (5.14). We follow the notation of ref. [36].

Within the eikonal approximation to u_{s}, we have, as $r\to\infty$,

$$\boldsymbol{p}u_{\mathrm{s}} \xrightarrow[r\to\infty]{} mv\gamma\hat{\boldsymbol{z}}u_{\mathrm{s}}. \tag{5.15}$$

Using eq. (5.15) in eq. (5.14), we obtain

$$\sigma_r = -\int_{s\to\infty}\mathrm{d}A\,u_{\mathrm{s}}^{\dagger}\hat{\boldsymbol{n}}\cdot\hat{\boldsymbol{z}}u_{\mathrm{s}}. \tag{5.16}$$

Since s is any large surface surrounding the interaction potential, we may take for it two planes perpendicular to the z-axis at $z=\pm\infty$. We then have

$$\sigma_{\mathrm{R}} = \int \mathrm{d}^2 b\,[|u_{\mathrm{s}}|^2(\boldsymbol{b}, z\to-\infty) - |u_{\mathrm{s}}|^2(\boldsymbol{b}, z\to+\infty)]. \tag{5.17}$$

Equation (5.17) exhibits very nicely the physical meaning of in terms of the probability densities $|u_{\mathrm{s}}|^2(\boldsymbol{b}, z\to-\infty)$ and $|u_{\mathrm{s}}|^2(\boldsymbol{b}, z\to+\infty)$.

Using the usual substitution for the upper component

$$u_{\boldsymbol{k},\mathrm{s}}^{(+)} = \mathrm{e}^{\mathrm{i}\boldsymbol{k}\cdot\boldsymbol{r}}\,\mathrm{e}^{\mathrm{i}S(r)}\chi_{\mathrm{s}}. \tag{5.18}$$

Here the χ_{s} are Dirac spinors and $S(\boldsymbol{r})$ satisfies the differential equation

$$\boldsymbol{k}\cdot\boldsymbol{\nabla}S(\boldsymbol{r}) = m[V_{\mathrm{c}}(r) + V_{\mathrm{so}}(r)(\boldsymbol{\sigma}\cdot\boldsymbol{r}\times\boldsymbol{k} - \mathrm{i}r\cdot\boldsymbol{k})]. \tag{5.19}$$

In equation (5.19) the central $V_c(r)$ and spin–orbit V_{so} interactions are given by [see eq. (5.11)]

$$V_c(r) = V_s(r) + \frac{E}{m} V_0(r) + \frac{V_s^2(r) - V_0^2(r)}{2m}, \tag{5.20}$$

$$V_{so}(r) = \frac{1}{2mA} \frac{1}{r} \frac{d}{dr} [V_0(r) - V_s(r)] \tag{5.21}$$

and $\boldsymbol{k} = \frac{1}{2}(\boldsymbol{k} + \boldsymbol{k}')$, the average of the initial and final momenta.

Defining the z-axis to be along the direction of $\boldsymbol{k}$, the eikonal phase $S(\boldsymbol{r})$ can be written as

$$iS(\boldsymbol{r}) = -\frac{m}{k} \int_{-\infty}^{z} dz' [V_c(b, z') + V_{so}(\boldsymbol{b}, z')(\boldsymbol{\sigma} \cdot \boldsymbol{b} \times \boldsymbol{k} - ikz')] . \tag{5.22}$$

Using eq. (5.22) in eq. (5.18), we can write down immediately

$$|u_s|^2(\boldsymbol{b}, z) = \chi_s^\dagger \exp[-2 \operatorname{Im} S(\boldsymbol{b}, z)] \chi_s . \tag{5.23}$$

We remind the reader that S is an operator in spin space.

Let us introduce the quantities

$$F = E - V_0(\boldsymbol{b}, z) , \tag{5.24}$$

$$N = m - V_s(\boldsymbol{b}, z) . \tag{5.25}$$

Then eqs. (5.17), (5.20) and (5.21) give us

$$\sigma_R = \chi_s^\dagger \left[\int d^2b \, (1 - e^{\phi(b)}) \right] \chi_s , \tag{5.26}$$

where

$$\phi(\boldsymbol{b}) = \phi_c(\boldsymbol{b}) - \phi_{so}(\boldsymbol{b}) \boldsymbol{\sigma} \cdot (\boldsymbol{b} \times \boldsymbol{k}) , \tag{5.27}$$

$$\phi_c(\boldsymbol{b}) = \frac{1}{(\hbar c)^2 k} \int_{-\infty}^{\infty} dz \operatorname{Im}(N^2 - F^2) , \tag{5.28}$$

$$\phi_{so}(\boldsymbol{b}) = b \int_{-\infty}^{\infty} dz \frac{1}{r} \operatorname{Im}\left(\frac{1}{F + N} \frac{\partial}{\partial r} (F + N) \right) . \tag{5.29}$$

At this point it is worth mentioning that the quantities $\phi_c(\boldsymbol{b})$ and $\phi_{so}(\boldsymbol{b})$ are related to the thickness functions $t_c(\boldsymbol{b})$ and $t_{so}(\boldsymbol{b})$ of Amado et al. [35, 36] defined by

$$t_c(b) = \frac{-i}{2(\hbar c)^2 k} \int_{-\infty}^{\infty} dz' (N^2 - F^2 + E^2 - M^2) , \tag{5.30}$$

$$t_{so}(b) = \frac{-ib}{2} \int_{-\infty}^{\infty} dz' \, \frac{1}{F+N} \, \frac{1}{r} \, \frac{\partial}{\partial r} (F+N) \, . \tag{5.31}$$

Thus

$$\phi_c(b) = 2 \, \mathrm{Re} \, t_c(b) \, , \tag{5.32}$$

$$\phi_{so}(b) = 2 \, \mathrm{Re} \, t_{so}(b) \, . \tag{5.33}$$

Going back to eq. (5.26), we note first that we can write it as

$$\begin{aligned} \sigma_R &= \chi_s^\dagger \Big(\int d^2b \, ([1 - e^{\phi_c(b)} \exp(-\phi_{so} \boldsymbol{\sigma} \cdot \hat{\boldsymbol{b}} \times \hat{\boldsymbol{k}})] \Big) \chi_s \\ &= \chi_s^\dagger \Big(\int d^2b \, [1 - e^{\phi_c(b)} \cosh \phi_{so}(b) + \boldsymbol{\sigma} \cdot (\hat{\boldsymbol{b}} \times \hat{\boldsymbol{k}}) \, e^{\phi_c(b)} \sinh \phi_{so}(b)] \Big) \chi_s \\ &= 2\pi \chi_s^\dagger \Big(\int b \, db \, [1 - e^{\phi_c(b)} \cosh \phi_{so}(b)] \Big) \chi_s = 2\pi \int_0^\infty b \, db \, [1 - e^{\phi_c(b)} \cosh \phi_{so}(b)] \, . \end{aligned} \tag{5.34}$$

The term involving $\boldsymbol{\sigma} \cdot \hat{\boldsymbol{b}} \times \hat{\boldsymbol{k}}$ does not contribute to the b-integral due to symmetry about the z-axis. Equation (5.34) can also be written as [see eqs. (5.32) and (5.33)]

$$\sigma_R = 2\pi \int_0^\infty b \, db \, (1 - \exp[2 \, \mathrm{Re} \, t_c(b)] \cosh [2 \, \mathrm{Re} \, t_{so}(b)]) \, . \tag{5.35}$$

Equation (5.35) is the principal result of this section. It expresses σ_R in the usual form of an impact parameter integral involving "relativistic" transmission coefficients given by

$$T(b) = 1 - \exp[2 \, \mathrm{Re} \, t_c(b)] \cosh[2 \, \mathrm{Re} \, t_{so}(b)] \, . \tag{5.36}$$

It is clear that the exact form and details of $T(b)$ would be irrelevant if the nucleon–nucleus scattering was dominated by a black-disk type absorption. In such a case $T(b)$ would be representable as

$$T(b) = \Theta(b - R_c) \, , \tag{5.37}$$

where $\Theta(x)$ is the step function, and R_c is a characteristic absorption radius. If eq. (5.37) is used σ_R becomes the simple geometrical limit,

$$\sigma_R = \pi R_c^2 \, . \tag{5.38}$$

If the above were true, not too much physics would be extracted from σ_R. Luckily total reaction cross-section data of proton–nucleus systems at intermediate energies exhibit major deviations from the black-disk result of eq. (5.38). Nuclei become quite transparent to nucleons at intermediate energies [2], and the quantity that measures this nuclear transparency in detail is given by $T(b)$ of eq. (5.36).

Therefore a detailed evaluation and discussion of $T(b)$ and the resulting σ_R is clearly called for. This has been done by Digiacomo, DeVries and Peng [2] using conventional nonrelativistic theory. In the following we present our result for and discussion of σ_R within the Dirac-eikonal treatment presented in this section.

Before presenting our results, we warn the reader that $t_c(b)$ is ill-defined for proton scattering because of the presence of the long-range Coulomb potential which is present in $V_0(r)$. This difficulty can be dealt with easily by some appropriate modification of the integral involved. The details are given in appendix I of ref. [23]. Here we only cite the final Coulomb-modified, but finite, σ_R

$$\sigma_R = 2\pi \int_0^\infty b\, db\, \{1 - \exp[2\,\mathrm{Re}\,\tilde{t}_c(b)]\cosh[2\,\mathrm{Re}\,t_{so}(b)]\}\,, \tag{5.39}$$

$$\tilde{t}_c(b) = \frac{-i}{2(\hbar c)^2 k} \int_{-\infty}^{\infty} dz \left(N^2 + F^2 + E^2 - m^2 - \frac{2EZ_1Z_2e^2}{r(b,z)}\right). \tag{5.40}$$

Finally, a word about the optical theorem and its generalized version for charged-particle scattering. For neutral particles the usual form of the optical theorem,

$$\sigma_R = \frac{4\pi}{k}\,\mathrm{Im}\,F(\boldsymbol{k},\boldsymbol{k};E) - \int |F(\boldsymbol{k},\boldsymbol{k}';E)|^2\, d\Omega_{k'}\,, \tag{5.41}$$

should yield the correct expression for σ_R. In fact, with the elastic scattering amplitude $F(\boldsymbol{k},\boldsymbol{k}';E)$ derived by Amado et al. [35, 36],

$$F(\boldsymbol{k},\boldsymbol{k}';E) = F_1 + \boldsymbol{\sigma}\cdot\hat{\boldsymbol{n}}F_2\,, \tag{5.42}$$

$$F_1 = -ik \int_0^\infty db\, bJ_0(qb)\{e^{t_c(b)}\cosh[t_{so}(b)] - 1\}\,, \tag{5.43}$$

$$F_2 = -k \int_0^\infty db\, bJ_1(qb)\, e^{t_c(b)}\sinh[t_{so}(b)]\,, \tag{5.44}$$

where $\boldsymbol{q} = |\boldsymbol{k} - \boldsymbol{k}'|$, and J_0 and J_1, are ordinary Bessel functions, eq. (5.42) results in exactly the expression for σ_R given in eq. (5.35).

For charged-particle scattering, eq. (5.41) yields infinite values for both terms on the rhs. However, a generalized optical theorem can be derived for this purpose and it does provide means of calculating σ_R,

$$\sigma_R = \frac{4\pi}{k}\,\mathrm{Im}[F(\boldsymbol{k},\boldsymbol{k};E) - F_C(\boldsymbol{k},\boldsymbol{k};E)] - \int [|F_C(\boldsymbol{k},\boldsymbol{k}';E)|^2 - |F(\boldsymbol{k},\boldsymbol{k}';E)|^2]\, d\Omega\,, \tag{5.45}$$

where F_C is the point Coulomb scattering amplitude. In a way, the procedure we employ amounts basically to calculating the difference $F - F_C$ in the form of an impact-parameter integral, which yields completely convergent results.

5.1. Numerical results

In what follows we present the results of our calculation of σ_R, eq. (5.39), for $p + {}^{40}Ca$ and $p + {}^{208}Pb$, in the proton energy range $10\,\text{MeV} < E_p < 1000\,\text{MeV}$. We take for the proton–nucleus optical potential the impulse-approximation Dirac optical interaction for spin-saturated nuclei in the general form [33, 34]

$$\langle k'|U_{00}|k\rangle = -(4\pi ik/m)[F_s(q)\rho_s(q) + \gamma_4 F_v(q)\rho_v(q)] \equiv V_s(q) + V_0(q)\,. \tag{5.46}$$

In eq. (5.46), F_s and F_v are the scalar and vector pieces of the Lorentz-invariant NN amplitude, respectively, and ρ_s and ρ_v are the scalar and vector form factors of the target nucleus, given by

$$\rho_s(q) = \langle 0|\sum_i e^{iq\cdot r_i}|0\rangle\,, \tag{5.47}$$

$$\rho_v(q) = \langle 0|\sum_i \gamma_4^i e^{iqr_i}|0\rangle\,. \tag{5.48}$$

The above densities can be better visualized when written in configuration space,

$$\rho_s(q) = \langle 0|\sum_i \gamma_4^i \delta(\boldsymbol{r} - \boldsymbol{r}_i)|0\rangle \equiv \sum_\alpha^{\text{occ.}} \bar{\psi}_\alpha(r)\psi_\alpha(r)\,, \tag{5.49}$$

$$\rho_v(r) = \langle 0|\sum_i \delta(\boldsymbol{r} - \boldsymbol{r}_i)|0\rangle \equiv \sum_\alpha^{\text{occ.}} \psi_\alpha^\dagger(r)\psi_\alpha(r)\,, \tag{5.50}$$

where we find α-sums are over occupied single-particle states. In terms of the upper and lower components,

$$\psi_\alpha = \begin{pmatrix} \psi_\alpha^U \\ \psi_\alpha^L \end{pmatrix}, \qquad \bar{\psi} = (\psi_\alpha^{U^*}, -\psi_\alpha^{L^*})\,, \tag{5.51}$$

we can express $\rho_s(r)$ and $\rho_v(r)$ as

$$\rho_s(r) = \sum_\alpha^{\text{occ.}} |\psi_\alpha^U(r)|^2 - \sum_\alpha^{\text{occ.}} |\psi_\alpha^L(r)|^2 \equiv \rho_U(r) - \rho_L(r)\,, \tag{5.52}$$

$$\rho_v(r) = \sum_\alpha^{\text{occ.}} |\psi_\alpha^U(r)|^2 + \sum_\alpha^{\text{occ.}} |\psi_\alpha^L(r)|^2 \equiv \rho_U(r) + \rho_L(r)\,. \tag{5.53}$$

Therefore the difference $\rho_v(r) - \rho_s(r)$ measures the strength of the lower component density $2\rho_L(r)$, and accordingly the degree to which the optical potential is relativistic.

The potential calculated by McNeil et al. [34] is obtained by setting $F_s(q) \simeq F_s(0)$ and $F_v(q) \simeq F_v(0)$ in eq. (5.46). In this limit, which is quite reasonable in the energy range considered, the Fourier transform of eq. (5.46) yields a local potential in configuration space, with its γ-dependence completely specified by $\rho_s(r)$ and $\rho_v(r)$. We therefore write

$$V_s(r) = V_s^0(E)\hat{\rho}_s(r) = [U_s^0(F) - iW_s^0(E)]\hat{\rho}_s(r)\,, \tag{5.54}$$

$$V_0(r) = V_0^0(E)\hat{\rho}_v(r) = [U_0^0(E) - iW_0^0(E)]\hat{\rho}_v(r)\,, \tag{5.55}$$

where $\hat{\rho}_s$ and $\hat{\rho}_v$ represent the shape of the densities and they are both normalized to unity in the central region. McNeil et al. [34] presented their results for $U_s^0(E)$, $W_s^0(E)$, $U_0^0(E)$ and $W_0^0(E)$ at a radius where ρ_s and ρ_v are both $0.16\,\mathrm{fm}^{-3}$. These values of the densities correspond to a final momentum, $k_F = 1.37\,\mathrm{fm}^{-1}$. It is found that W_s^0 is negative, implying, using our convention in eq. (5.2), that the scalar interaction is regenerative whereas the vector one is absorptive. Their values come out comparable, with $W_0^0(E)$ a bit larger than W_s^0. All of these results are in accord with phenomenological findings. The above results were also confirmed by Horowitz [37] in his nuclear-matter calculation of W_s and W_0.

Armed with the above facts we evaluated σ_R of eq. (5.39), using the results of McNeil et al. as presented in their fig. 1. For the density shape of ^{208}Pb we have used Wood–Saxon forms with parameters fixed in accordance with results obtained from electron scattering, which basically supplies ρ_v for protons. We have, however set $\hat{\rho}_s(r) = \hat{\rho}_v(r)$ for all r. The radius R and diffuseness a parameters for ^{208}Pb, are [2] $R = 6.624\,\mathrm{fm}$, $\alpha = 0.549\,\mathrm{fm}$.

The density shape of ^{40}Ca is usually parametrized as

$$\hat{\rho}_{^{40}\mathrm{Ca}}(r) = (1 + \omega r^2/R^2)[1 + \exp(r - R)/a]^{-1}\,, \tag{5.56}$$

with $\omega = 0.1017$, $R = 3.669\,\mathrm{fm}$, $a = 0.584\,\mathrm{fm}$.

The results are presented in figs. 14 and 15*). It is clear from the figures that the agreement of our σ_R in the energy range $100\,\mathrm{MeV} < E < 1000\,\mathrm{MeV}$ with the data [2] is as good as the one obtained with the nonrelativistic theory. This finding convinces us that our calculation of σ_R for heavy ions presented in this paper, with the conventional nonrelativistic $t\rho_1\rho_2$ potential should be adequate.

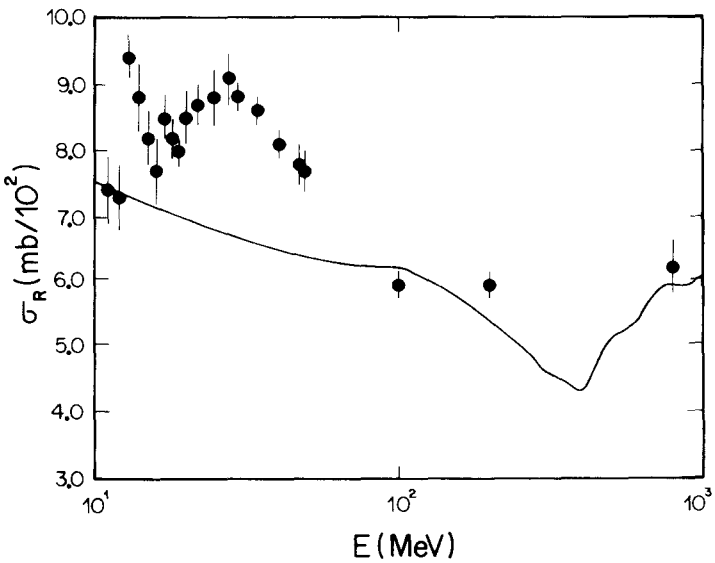

Fig. 14. Total reaction cross section for p + ^{40}Ca calculated with the relativistic Dirac description. The data points were taken from the references cited in ref. [23].

*) The p + ^{40}Ca and p + ^{208}Pb were collected from several references; see ref. [23].

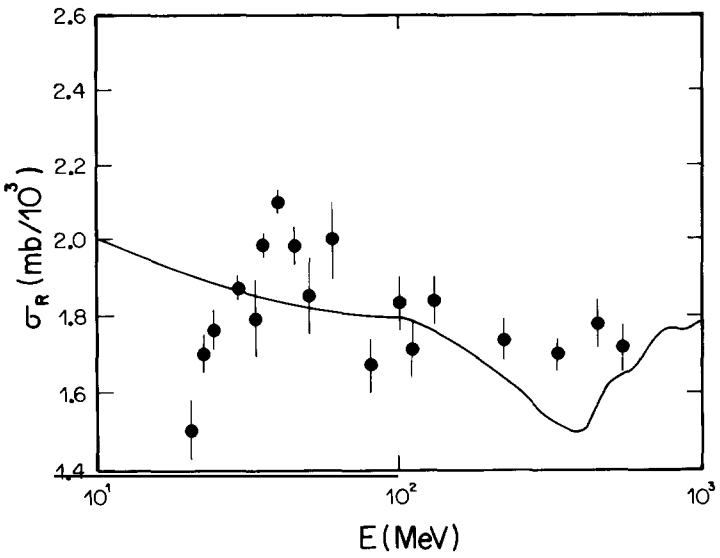

Fig. 15. Same as fig. 14 for p + ^{208}Pb.

6. Calculation of σ_R for several heavy-ion systems

Having obtained the microscopic ion–ion potential in the previous sections, we are now in a position to test it insofar as its reactive content is concerned. Further, the range of dominance in W of inclusive single-nucleon knockout at intermediate energies can now be assessed. In this section we present a detailed account of our calculation of the total reaction cross section, σ_R, for several heavy-ion systems. In particular we discuss the degree of transparency in these systems and how this is related to the mean free path, as discussed qualitatively in section 2. Another related question which is addressed here is the dependence of σ_R on the effective radius of the system and how this dependence changes with energy. In our calculation, we also include the second-order double NN scattering potential discussed in section 3.

The expression we use for σ_R is the WKB one given in eqs. (2.13), (2.17) and (2.21), namely,

$$\sigma_R = 2\pi \int b\, db\, \{1 - \exp[-4\delta_I(b)]\}\,, \tag{6.1}$$

with $\delta_I(b)$ given by eq. (2.19), and evaluated for the $t\rho_1\rho_2$ potential discussed in the section 3, with the Pauli blocking effects fully incorporated as done in section 4. The expression we use for σ_R contains the effect of refraction arising from the real part of the heavy-ion interaction potential [3]. It also contains an improvement over the treatment of other authors in that we include, besides the usual nuclear-medium corrections, the second-order double scattering component discussed in section 3.

We have calculated σ_R for several heavy-ion systems, ranging from light, such as the very extensively studied ^{12}C + ^{12}C, to the very heavy ^{208}Pb + ^{208}Pb. Our aim in this, is not so much the reproduction of the existing data, but rather to pin down the energy region in which the $t\rho\rho$ interaction approximates well the complex ion–ion potential, with its reactive content being predominantly single- and double-nucleon knockout (single knockout and double knockout being, respectively, associated with the

imaginary parts of the single scattering $t\rho_1\rho_2$ and double scattering $(t\rho_1)^2\rho_2$ interactions). We shall see that, at low energies where Pauli blocking greatly reduces the strength of the imaginary part, as that seen in the previous chapter, the total reaction cross section calculated according to eq. (6.1) becomes much smaller than is obtained from the data; this should be expected since no account is taken of nuclear surface inelastic excitation, fusion and other processes which dominate σ_R at these energies.

In fig. 16 we present the result for $^{12}C + {}^{12}C$. The solid curve represents the result obtained with eq. (4.1), including the Coulomb and the real part of the nuclear potentials. In the energy range $100\,\text{MeV/N} < E_{CM}/A < 800\,\text{MeV/N}$ the agreement with the data is reasonable. At lower energies, however, our calculation underestimates the data by a factor which could be as large as 2 at $E_{CM} \sim 10\,\text{MeV}/A$. The dashed curve represents the result without V_N and V_C and with no Pauli blocking. The fact that this curve approximates very well the data is clearly fortuituous. The crosses shown represent the result of nuclear matter calculation reported by Faessler et al. [4]. This calculation seems to come close to our calculation when Pauli blocking is taken into account, but with neither V_N nor V_C (shown as the dashed–dotted line). It is important to notice that both Pauli blocking and nuclear + Coulomb refractive effects are quite insignificant at higher energies. Thus it is in the low energy regime that the theory gets its major check. Of course it is exactly at these energies where other nuclear processes, not accounted for by the $t\rho\rho$ interaction, start coming into play, as already discussed. These processes gradually fill in the gap between the calculated microscopic σ_R and the data. Of these incomplete fusion and deep inelastic processes are probably the most important at $5\,\text{MeV/N} < E/A < 15\,\text{MeV/N}$, followed by complete fusion. Inelastic and transfer reactions as well as other quasi-elastic processes always contribute with varying weights, depending on the energy.

We have also calculated σ_R for other systems. In figs. 17–24, we show our results for $^{12}C + {}^{40}Ca$, $^{40}Ca + {}^{40}Ca$, $^{12}C + {}^{90}Zr$, $^{90}Zr + {}^{90}Zr$, $^{12}C + {}^{208}Pb$, $^{40}Ca + {}^{208}Pb$, $^{90}Zr + {}^{208}Pb$ and $^{208}Pb + {}^{208}Pb$. These

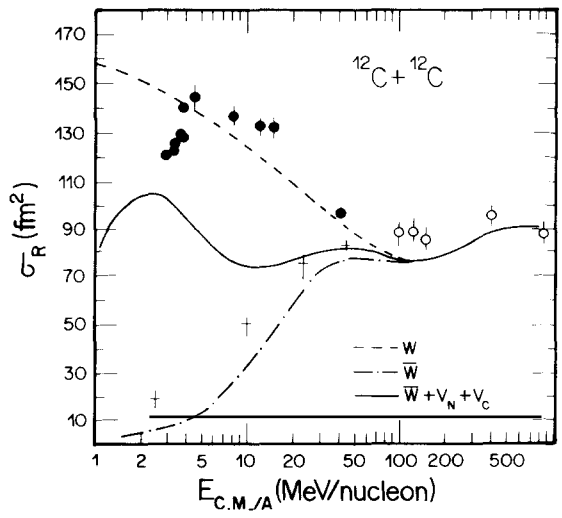

Fig. 16. The total reaction cross section for $^{12}C + {}^{12}C$ versus E_{CM}/A. The solid curve includes Pauli blocking plus refractive effects, the dashed–dotted curve corresponds to $\bar{\sigma}$ with *no* refractive effects, and the dashed curve represents calculation with the free σ_T^{NN}. The data points were collected from the experimental papers cited in the reference list (refs. [7–10]).

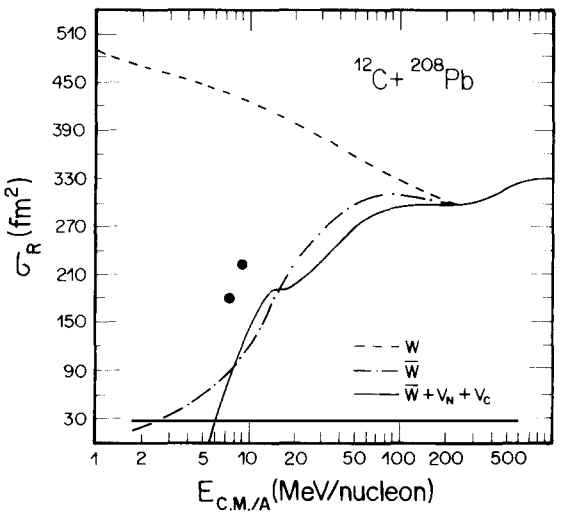

Fig. 17. Same as fig. 16 for $^{12}C + {}^{208}Pb$.

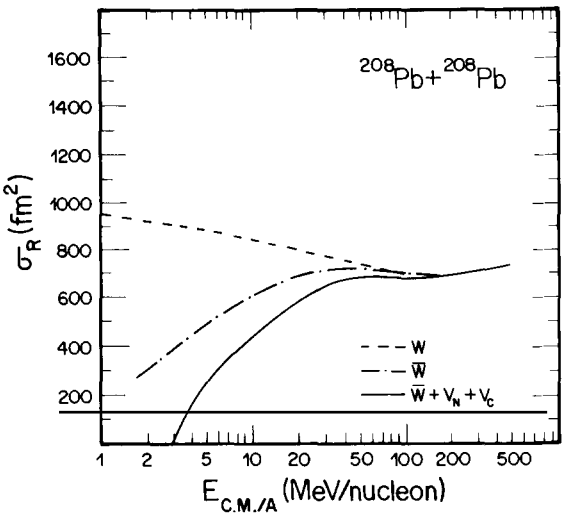

Fig. 18. Same as fig. 16 for ^{208}Pb + ^{208}Pb.

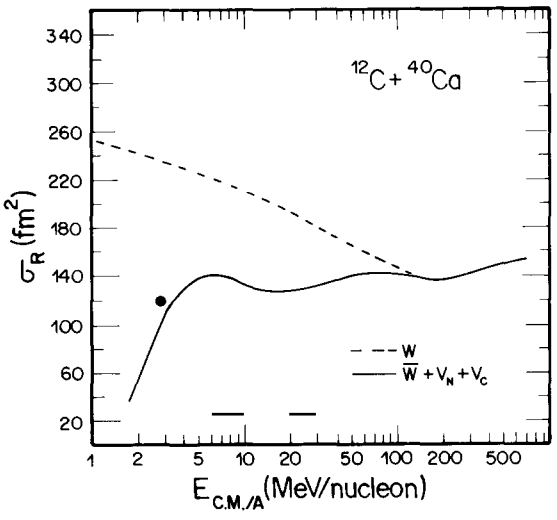

Fig. 19. Same as fig. 16 for ^{12}C + ^{40}Ca (no calculation with $\bar{\sigma}$ is shown; see text for details).

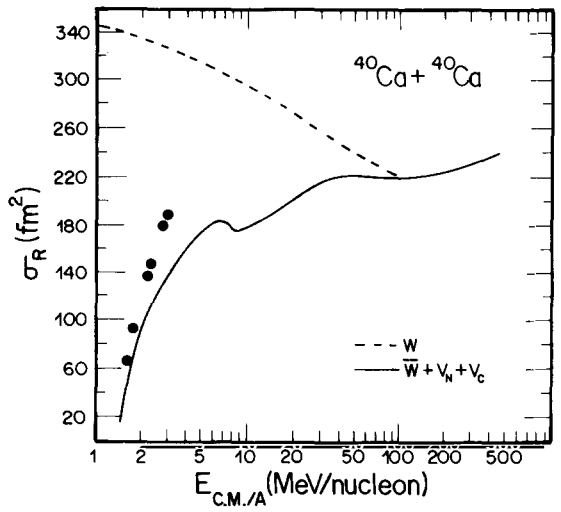

Fig. 20. Same as fig. 16 for ^{40}Ca + ^{40}Ca.

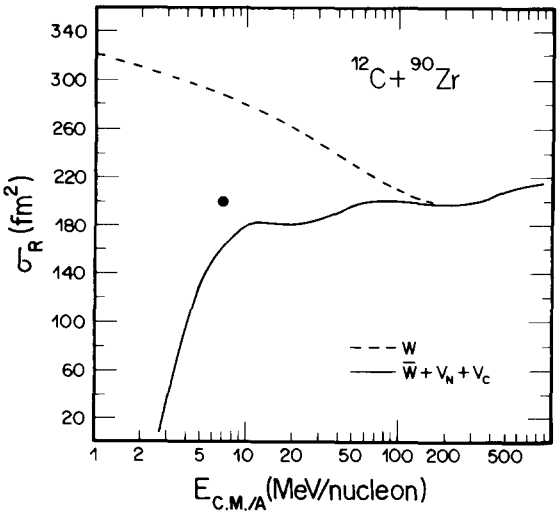

Fig. 21. Same as fig. 16 for ^{12}C + ^{90}Zr.

systems were chosen to represent different mass regions. In some cases few data points exist, in others, none. In all cases, we see the clear drop in σ_R (solid curves) as the energy is lowered, indicating the approach to the threshold of the processes described by the $t\rho_1\rho_2$ interaction. Further, the small dip in σ_R close to the effective threshold for single pion production in the nucleon–nucleon scattering becomes less conspicuous as the mass of the heavy-ion system increases.

Having calculated microscopically the total reaction cross section from the $t\rho_1\rho_2$ interaction, it is now possible to evaluate the degree of transparency in the different HI systems at intermediate energies. Before doing this, it is useful to establish first the connection between our calculated results for σ_R and

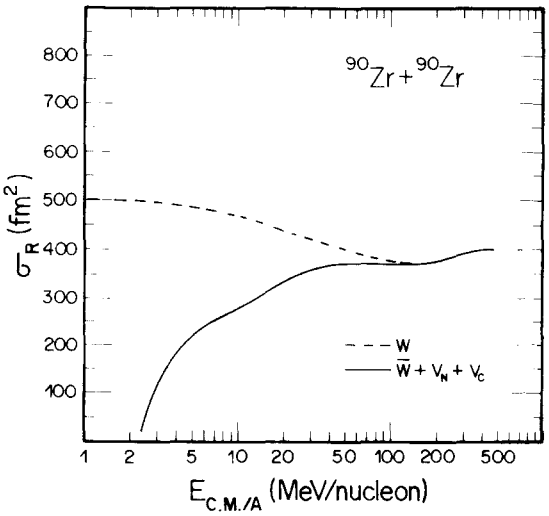

Fig. 22. Same as fig. 16 for $^{90}Zr + ^{90}Zr$.

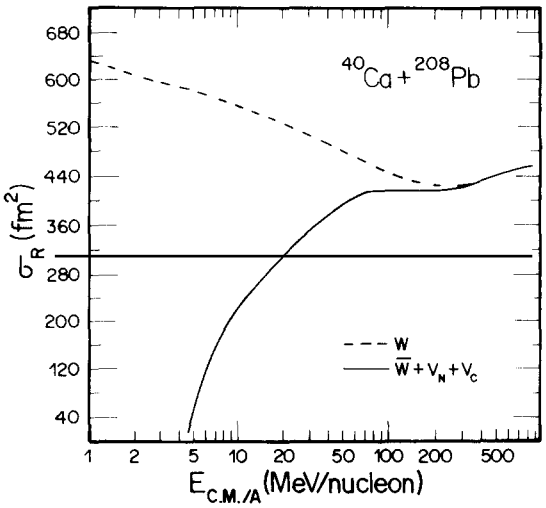

Fig. 23. Same as fig. 16 for $^{40}Ca + ^{208}Pb$.

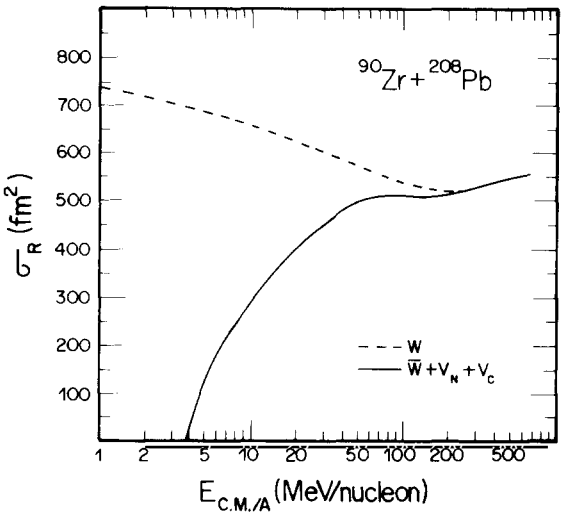

Fig. 24. Same as fig. 16 for $^{90}Zr + ^{208}Pb$.

the geometrical formula given by eq. (2.16),

$$\sigma_R = \pi R^2 (1 - V_B/E_{CM}) . \tag{6.2}$$

We considered the systems $^{12}C + ^{208}Pb$, $^{40}Ca + ^{208}Pb$, $^{90}Zr + ^{208}Pb$ and $^{208}Pb + ^{208}Pb$ at $E_{CM}/A = 10$, 200, 400 and 600 MeV/N. To reproduce the theoretical values of σ_R with eq. (5.2), we were forced to use the following small values of the radius parameter r_0 [$R = r_0(A_1^{1/3} + A^{1/3})$]: 1.22, 1.26, 1.26, and 1.26 fm, respectively, for the four systems mentioned above.

These values for r_0 are considerably smaller than what one might expect if the geometrical limit of σ_R had been reached by these systems. Such a limit is usually specified by the strong absorption radius which gives $r_0 = 1.5$ fm. In fact to reproduce the available $^{12}C + ^{12}C$ data, shown in fig. 14 at

$E_{CM}/A \simeq 5$ MeV/N, we need to use $r_0 = 1.57$ fm. It is therefore clear that these systems do exhibit a large degree of transparency T (eq. 2.27) as was suggested by several authors. However, one has to be careful when assessing this transparency since there is a strong dependence on the value of r_0 used. For example according to Bohlen et al. [9] there is a 12% transparency in $^{12}C + {}^{12}C$ at $E_{CM}/A = 12$ MeV/N whereas De Vries et al. [2] predict a zero value for T. Such a discrepancy stems from the fact that these authors use different values for the strong-absorption radius parameter in eq. (6.12).

We present now our calculation of T, based on our theoretical results, which we compare to the equation

$$\sigma_R = \pi R_B^2 (1 - V_B/E_{CM})(1 - T)\,, \tag{6.3}$$

with a radius parameter r_0, of about 1.5 fm. For the $^{12}C + {}^{12}C$ system this parameter is slightly larger ($r_0 = 1.57$). In table 2 we show our results for $^{12}C + {}^{12}C$, $^{12}C + {}^{208}Pb$, $^{40}Ca + {}^{40}Ca$ and $^{208}Pb + {}^{208}Pb$ at $E_{CM}/A = 50$, 100, 200 300 and 500 MeV/N. We see clearly that the transparency factor ranges in value from about 50% for the lightest system to about 27% for the heaviest one.

In our calculation of σ_R presented so far, we did not take into account the effect of statistics in the identical projectile–target systems. We now discuss this point, and present estimates of the effect. The elastic scattering amplitude $f(\theta)$ should be written as

$$\overline{f(\theta)} = f(\theta) + \tau(-)^{2I-s} f(\pi - \theta) \tag{6.4}$$

where $\tau = +(-)$ for boson (fermions), I is the intrinsic spin of the partners and s denotes the channel spin $s = 0, 1, 2, \ldots, 2I$. In what follows we take the case of two bosons with $I = 0$ (e.g., ^{12}C). Thus, through the application of the optical theorem to $\overline{f(\theta)}$, and with $P_l(\theta) = (-)^l P_l(\pi - \theta)$, we obtain

$$\bar{\sigma}_R = \frac{\pi}{k^2} \sum_l^{\infty} (2l + 1)[1 + (-)^l] T_l\,, \tag{6.5}$$

which can be written, in the impact parameter representation, as

$$\bar{\sigma}_R(E) = 2\pi \int_0^{\infty} db\, b[1 + \cos(kb - \tfrac{1}{2})] T(b)\,, \tag{6.6}$$

where we have used $(-1)^l = \cos \pi l$ and $l + \frac{1}{2} = kb$.

Table 2
The percentage transparency for $^{12}C + {}^{12}C$, $^{12}C + {}^{208}Pb$, $^{40}Ca + {}^{40}Ca$ and $^{208}Pb + {}^{208}Pb$, at several center-of-mass energies; see text for details

$^{12}C + {}^{12}C$ [a]		$^{12}C + {}^{208}Pb$ [b]		$^{40}Ca + {}^{40}Ca$ [b]		$^{208}Pb + {}^{208}Pb$ [b]	
$\frac{E_{CM}}{A}\left(\frac{\text{MeV}}{\text{nucleon}}\right)$	T	$\frac{E_{CM}}{A}\left(\frac{\text{MeV}}{\text{nucleon}}\right)$	T	$\frac{E_{CM}}{A}\left(\frac{\text{MeV}}{\text{nucleon}}\right)$	T	$\frac{E_{CM}}{A}\left(\frac{\text{MeV}}{\text{nucleon}}\right)$	T
50	46.7%	50	34.4%	50	28.9%	50	26.2%
100	50.9%	100	32.2%	100	32.4%	100	29.1%
200	49.0%	200	35.4%	200	31.1%	200	28.2%
300	47.8%	500	32.9%	300	30.0%	300	27.1%
500	44.0%	900	25.2%	500	27.2%	500	25.5%

[a] $r_0 = 1.57$ fm. [b] $r_0 = 1.50$ fm.

Table 3
The identical-particle correction of the total reaction cross sections of the systems $^{12}C + {}^{12}C$, $^{40}Ca + {}^{40}Ca$, $^{90}Zr + {}^{90}Zr$ and $^{208}Pb + {}^{208}Pb$; see text for details

E_{Lab}/A	$^{12}C + {}^{12}C$		$^{40}Ca + {}^{40}Ca$		$^{90}Zr + {}^{90}Zr$		$^{208}Pb + {}^{208}Pb$	
(MeV/N)	b_c (fm)	$\Delta\sigma_s$ (fm^2)	b_c	$\Delta\sigma_s$ (fm^2)	b_c	$\Delta\sigma_s$ (fm^2)	b_c	$\Delta\sigma_s$ (fm^2)
2	5.5	−8.56	5.0	−4.28	5.0	−0.03	4.0	0.44
4	5.5	12.28	5.0	−2.24	5.0	−0.85	4.0	−0.37
6	5.5	−11.29	6.5	0.14	6.5	−1.29	4.0	0.27
8	5.5	7.97	7.0	−3.46	7.0	−0.61	6.0	0.44
10	5.5	−3.4	7.0	2.71	8.0	−0.52	8.5	0.74
12	5.5	−4.49	7.0	−2.75	8.5	0.46	9.0	−0.69
14	5.5	6.72	7.0	2.23	8.5	−1.45	9.5	−0.46
16	5.5	−1.07	7.5	−2.53	9.0	1.31	10.0	−0.69
18	5.5	−6.09	7.5	1.15	9.0	1.35	11.0	−0.48
20	5.5	2.11	7.5	2.37	10.0	−0.19	12.0	0.72
22	5.5	4.6	8.0	0.89	10.0	1.2	15.0	0.54
24	5.5	3.8	8.0	1.45	12.0	−1.12	15.0	0.42

Let us now evaluate the above expression in the sharp cut-off model, namely,

$$T(b) = \Theta(b_c - b)\,, \tag{6.7}$$

where b_c is the Coulomb modified sharp cut-off radius. Then

$$\bar{\sigma}_R(E) = \sigma_R(E) + \Delta\sigma_{stat}\,, \tag{6.8}$$

$$\sigma_R(E) = \pi b_c^2\,, \tag{6.9}$$

$$\Delta\sigma_{stat} = 2\pi\{(b_c/\pi)\sin(kb_c - \tfrac{1}{2}) + (1/k^2)[\cos(kb_c - \tfrac{1}{2}) - \cos(\tfrac{1}{2})]\}\,. \tag{6.10}$$

In the above expression $\Delta\sigma_{stat}$ represents the correction to σ_R arising from the identity of the particles.

In table 3 we present the values of $\Delta\sigma_{stat}$ for several identical heavy-ion systems at several CM energies per nucleon. We see clearly that $\Delta\sigma_{stat}$ contributes at most about 5% at these energies. At higher energies the effect is even smaller. Thus, for all practical purposes, we can ignore $\Delta\sigma_{stat}$. The use of the more realistic $T(b)$ in eq. (6.1) does not change appreciably the above conclusions.

In the next section we turn our attention to the case of exotic (neutron- and proton-rich) nuclei. The study of these nuclei has intensified considerably in the last several years and a summary of some relevant facts is in order, particularly what concerns the total reaction cross section.

7. Reactions with radioactive secondary beams

Some nuclear fragments originating from heavy-ion scattering at high energies are formed from a piece of the projectile nucleus that has not been scraped off by the target. Such fragments tend to keep various properties that the projectile nucleus had before the collision. For example, they have almost the same velocity as the beam velocity. As regards the neutron-to-proton ratio N/Z, heavy-mass projectiles such as ^{238}U contain more neutrons than protons ($N/Z = 1.6$ for U). On the other hand, the

stability line of nuclei extends along $N/Z = 1$ for light nuclei. Therefore, light-mass projectile fragments from U beams tend to fill the unstable neutron-rich region.

Following this idea, several new neutron-rich isotopes lasting a short period of time were discovered at the BEVALAC accelerator [38–40]. One interesting application of these isotopes is their usage as secondary beams. Since the velocities of these isotopes are almost equal to the beam velocity, high-quality secondary beams are expected. Recently, a Japanese group [41] has extensively investigated and measured the inteaction cross sections of secondary beams at the BEVALAC, following this technique. Such experiments have also been performed at GANIL with intermediate-energy beams [42, 43].

In this chapter we make a brief analysis of the reaction cross sections involving radioactive secondary beams. An important motivation for these measurements is to determine the size of neutron-rich nuclei.

By comparing the experimental data with the geometrical area $\sigma = \pi(R_P^2 + R_T^2)$, with R_P (R_T) equal to the projectile (target) radius, one finds [41] that the radii of ^{11}Li, ^{12}Be and ^{14}Be are much larger than expected from the standard formula $R_i = 1.2A^{1/3}$ fm. Sato and Okuhara [44] and Bertsch, Brown and Sagawa [45] have shown that these reaction cross sections for light nuclei can be calculated quite well with the approximations of the Glauber model, which is given, e.g., for a zero-range nucleon–nucleon interaction, by [see eqs. (6.1) and (3.23)]

$$\sigma_R = 2\pi \int b\, db \left[1 - \exp\left(-\sigma_{NN} \int d^3 r_1 \rho_z^{(P)}(|r_1|)\rho_z^{(T)}(|r_1 - b|)\right)\right],$$
$$\rho_z(r) = \int dz\, \rho(\sqrt{r^2 + z^2}). \tag{7.1}$$

The densities are determined from the Hartree–Fock single-particle wavefunctions combined with the shell-model occupation probabilities [45]. The result of this calculation is shown in figs. 25–27 where the isotopic dependence of σ_R is shown. The energy dependence σ_R for the cases shown, namely Li and Be, is completely determined by that of σ_{NN}, as already emphasized earlier in the report.

The situation becomes complicated if the target is a nucleus with a large Z. In this case, the Coulomb interaction between projectile and target plays an important role. In fact, Coulomb excitation of giant resonances is a relevant part of the reaction cross section already for intermediate-energy nuclear collisions [46]. Bertulani and Baur [47] have studied extensively the implications of the Coulomb interaction in high energy collisions. For relativistic energies the cross sections for Coulomb excitation of giant resonances may even be larger than the geometrical cross sections. Since the giant resonances decay mainly through particle emission, or by fission, the relevance of such processes to the computation of total reaction cross sections is obvious.

Not only the coherent action of the Coulomb field becomes important in high energy collisions. Also, the coherent action of the nuclear field leads to new effects in peripheral collisions at high energies. The effect of emission of correlated nucleons was studied among others in refs. [48, 49].

We shall not enter into the details of the effects of the coherent action of the nuclear and Coulomb fields in peripheral collisions at high energies. But, due to their large contribution to the total reaction cross sections, it is worthwhile to show examples of their applications. Being a rapidly growing field, the reactions with radioactive secondary beams offer a good opportunity for this (see ref. [50]).

Besides the measurements of the reaction cross sections with radioactive secondary beams, another intriguing experimental result is related to the momentum distribution of the ^{9}Li fragments originating

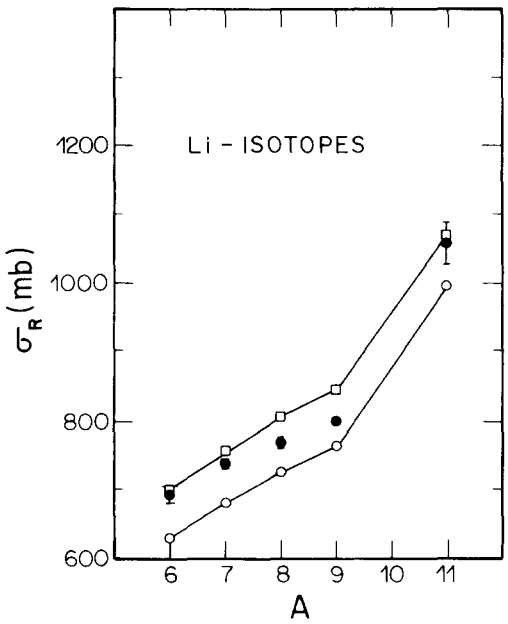

Fig. 25. Total reaction cross section for Li isotopes on ^{12}C at $E/A = 800$ MeV/N. See text for details. The data points were taken from ref. [41].

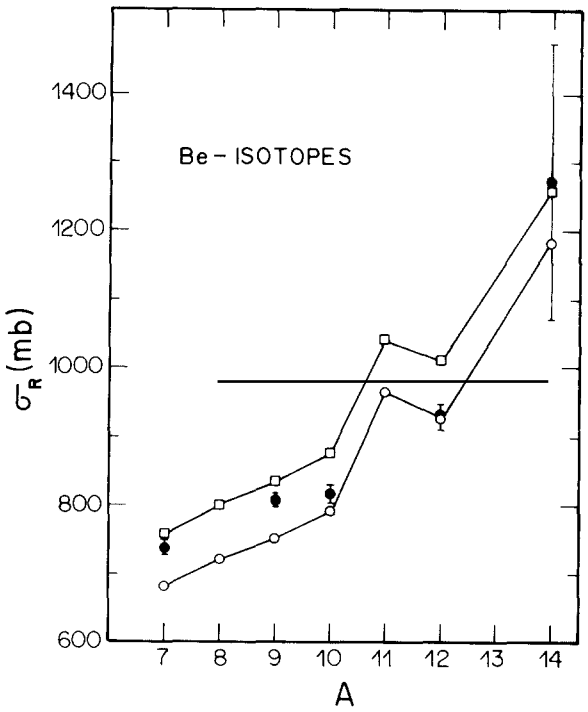

Fig. 26. Same as fig. 25 for Be isotopes.

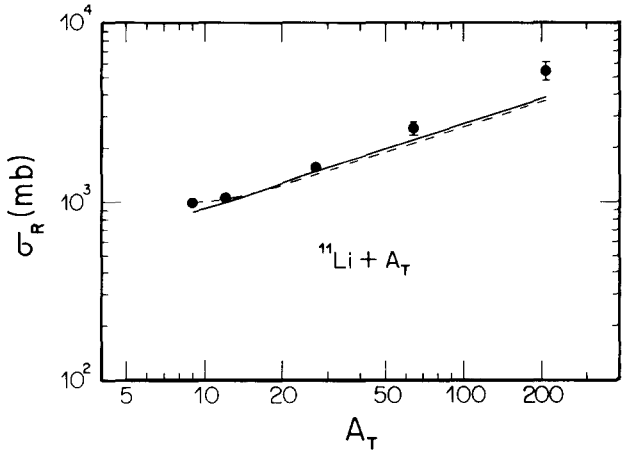

Fig. 27. Total reaction cross section of ^{11}Li on several targets at $E/A = 800$ MeV/N. The data points were taken from ref. [41].

from the reaction $^{11}Li + \text{target} \rightarrow {}^{9}Li + X$. These fragments result from peripheral reactions and give information about the nuclear matter distribution near the surface of the ^{11}Li isotope. The perpendicular momentum distribution of the ^{9}Li fragments shows a "two-peak" structure [41], with a narrow peak on top of a wider one. The widths of gaussian fits to these peaks are given by $\sigma_{\text{wide}} = 95 \pm 12$ MeV/c for the wider peak, and $\sigma_{\text{narrow}} = 23 \pm 5$ MeV/c for the narrower one. Such structure has also been found in

the reaction ^{14}Be + target$\rightarrow$ ^{12}Be + X. In the case of ^{11}Li it is known that the separation energy of the last two neutrons is $S_{2n} = 0.19 \pm 0.10$ MeV, while the separation energy of only one nucleon is as much as $S_{1n} = 0.96 \pm 0.1$ MeV.

Hansen and Jonson [51] have argued that it is the strength of the neutron pairing which is responsible for the differences in the separation energies of ^{11}Li and of other neutron-rich nuclei. This pairing makes the bond between the two loosely bound neutrons much stronger than the respective bonds between each of them and the ^{9}Li core. That is, the ^{11}Li is much like a cluster nucleus with a di-neutron system bound to the ^{9}Li core. It is the aim of this paper to show that both the widths of the momentum distributions as well as the total cross sections can be explained by assuming a simple cluster-like structure for ^{11}Li as a di-neutron bound to a ^{9}Li core. But we also show that analogous results can be obtained by considering the excitation of a soft vibration of the protons against the neutrons in ^{11}Li. The presently available data do not unambiguously distinguish between the two models.

Due to the small energy necessary to remove the neutron pair, the reaction process is of peripheral nature. The fragmentation is then originated by the nuclear field when the tails of the nucleonic distributions just touch each other, or by the Coulomb field even when the nuclei pass several tens of fermis far from each other. The scattering angle θ is therefore very small, and the momentum transfer in the reaction Δp is related to energy transfer by

$$\Delta p = p_f \cos\theta - p_i \cong E^*/v\,, \tag{7.2}$$

where v is the projectile velocity. Since the energy E^* transferred in peripheral processes is typically of the order of a few MeV, it cannot be absorbed by a single nucleon. The nucleon would carry a momentum $\sim\sqrt{2mE^*}$, which is appreciably larger than that of eq. (7.2) for $v \sim c$. However, such energy could be absorbed by a nucleon pair, or a pair of clusters, which can have high kinetic energy and small total momentum when the nucleons move in approximately opposite directions. Relation (7.2) can also be satisfied if collective excitations, like vibrational modes, are excited.

Let us assume that the energy E^* deposited in the nucleus with mass number A leads to its fragmentation into two pieces which fly apart with opposite momenta having the same magnitude p. If one of the fragments have mass number a, the following relations holds:

$$E^* - \varepsilon = p^2/2(A-a)m_N + p^2/2am_N\,, \tag{7.3}$$

where m_N is the nucleon mass and ε is the binding energy between the two clusters. The momentum widths of the fragments are obtained, after averaging (7.3), by

$$\langle p^2\rangle = 2m_N\langle K\rangle a(A-a)/A\,, \tag{7.4}$$

where $\langle K\rangle = \langle E^*\rangle - \langle\varepsilon\rangle$ is the average kinetic energy of the fragments.

This formula is very much like the one obtained by Goldhaber [52] for the momentum width of a fragment having mass number a resulting from the fragmentation of a nucleus of mass number A. No wonder, because both approaches rely on momentum and energy conservation. Goldhaber assumes that the momentum width results from an average of the net momentum obtained by adding the individual momenta of the nucleons inside the fragment at the exact moment it flies off the nucleus. This procedure realates $\langle p^2\rangle$ to the Fermi momentum P_F of nucleus A. The final result (which assumes $\langle E^*\rangle \sim 0$) is eq. (7.4) with $2m_N\langle K\rangle$ replaced by $P_F^2/5$.

Since the transferred energy depends on the specification of the target, as well as on the beam energy, then by means of a variation of these parameters the measurement of $\langle p^2 \rangle$ yields precious information about $\langle \varepsilon \rangle$. In the case of $^{11}\mathrm{Li} \rightarrow {}^{9}\mathrm{Li} + 2\mathrm{n}$, the narrow peak with width $\langle p^2 \rangle^{1/2} = 23 \pm 5\,\mathrm{MeV}/c$, gives $\langle K \rangle = 0.17 \pm 0.08\,\mathrm{MeV}$, while for the wide peak with width $\langle p^2 \rangle^{1/2} = 95 \pm 12\,\mathrm{MeV}/c$ one obtains $\langle K \rangle = 2.9 \pm 0.8\,\mathrm{MeV}$. Since the binding energy ε of any pair of neutrons in ^{11}Li cannot be larger than several MeV (one could imagine that at least one of the neutrons comes from the inner part of ^{11}Li, where it is more tightly bound), the above results show that the energy E^* transferred in the process cannot be larger than several MeV, too. This means that the dissociation is very soft and occurs at very large impact parameters, probing the tail of the nuclear matter distribution in ^{11}Li. The average kinetic energy $\langle K \rangle$ associated with the narrow peak is of the same magnitude as the binding energy of the loosely bound neutrons. Then, it may give information about the correlation distance between the di-neutron system and the ^{9}Li core, within the cluster-like hypothesis. On the other hand, the wider peak reveals that a more tightly bound neutron is taken out of ^{11}Li. An analysis of the dissociation cross section as a function of the relative final momentum of the fragments confirms the above hypothesis, as we show next.

Assuming that the ^{11}Li possesses a binary cluster structure (di-neutron + ^{9}Li), one can make simple estimates of the cross sections for its dissociation. Using a deuteron-like wavefunction for the pair of clusters and a strong absorption model, simple expressions were obtained in ref. [53]. The nuclear contribution to the differential cross section, in the limit $q \rightarrow 0$, is obtained as

$$\mathrm{d}\sigma_{\mathrm{N}}/\mathrm{d}q \cong R_{\mathrm{T}}\, q^2/(\eta^2 + q^2)^2\,, \tag{7.5}$$

where q is the relative momentum of the clusters after the dissociation, R_{T} is the target radius, and $\eta = \sqrt{2\mu\varepsilon}/\hbar$, with μ equal to the reduced mass of the clusters.

The Coulomb contribution to the differential cross section (taking only the E1-multipole contribution) in the same limit, is given by

$$\frac{\mathrm{d}\sigma_{\mathrm{C}}}{\mathrm{d}q} = \tfrac{128}{3} Z_{\mathrm{T}}^2 \alpha \left(\frac{c}{v}\right)^2 \left(\frac{Z_1 A_2 - A_1 Z_2}{A}\right)^2 \frac{\eta q^4}{(\eta^2 + q^2)^4} \left[\ln\left(\frac{\gamma v}{\delta w R}\right) - \frac{v^2}{2c^2}\right], \tag{7.6}$$

where $\gamma = (1 - v^2/c^2)^{-1/2}$ is the relativistic Lorentz factor, $\delta = 0.891$ and $\hbar w = \hbar^2(\eta^2 + q^2)/2\mu$. A_i (Z_i) refers to the mass (charge) number of cluster i ($A = A_1 + A_2$) and $R = R_{\mathrm{T}} + R_{\mathrm{P}}$.

The above expressions reveal that the spread in q^2 is of order of $\langle q^2 \rangle \cong \eta^2$. This means that the relative kinetic energy of the clusters after the dissociation has on the average the same value as their binding energies. This is indeed what we obtained above for $\langle K \rangle$ associated with the narrow momentum component. Therefore, the narrow momentum component can be interpreted as originating from the removal of two neutrons weakly bound in ^{11}Li. The root mean square radius for ^{11}Li, supposed to be a deuteron-like system, is $\langle r^2 \rangle^{1/2} = 1/\sqrt{2}\eta \sim 5.8\,\mathrm{fm}$. Th experimental value [41] for the rms radius of the ^{9}Li core is about 2.5 fm. Therefore, the di-neutron system forms a neutron *halo* around the ^{9}Li core.

As has been pointed out by Tanihata [55] the amount of kinetic energy associated with the broad momentum width (~3 MeV) is related to the binding energy of neutrons in the ^{9}Li core. As in the case of ^{9}Li + 2n described above, a pair of neutrons in the ^{9}Li core can also absorb the transferred energy in the reaction with the final relative momentum and energy obeying eq. (7.2). In this case the decay constant η in eqs. (7.5) and (7.6) can be related to the average binding energy of neutrons in the ^{9}Li

core as $\eta = \sqrt{m_N \varepsilon_c}/\hbar$. Taking $\varepsilon_c \sim 3$ MeV, this yields a rms radius of about 2.65 fm, which agrees very well with the rms radius of ^{9}Li.

Neutrons coming out of the ^{9}Li core can also have their origin in its collective excitation. The most effective way of creating such excitations is by means of the Coulomb interaction. It gives the same "kick" to all Z protons inside ^{9}Li, leading to their collective motion. For collisions with impact parameter b, this kick leads to an energy transfer which can easily be calculated as [55]

$$\Delta E_1 = 2Z(Z_T e^2)^2/m_N b^2 v^2 ,$$

where Z_T is the target charge. But the protons are not free and they pull the neutrons together. This leads to a movement of the whole nucleus, and the Coulomb recoil that one obtains by assuming that the nucleus with mass number A is a rigid body is

$$\Delta E_2 = 2(ZZ_T e^2)^2/Am_N b^2 v^2 .$$

The difference between these energies goes to the vibration of the Z protons against the N neutrons, and is

$$E^* = \Delta E_1 - \Delta E_2 = 2(NZ/A)(Z_T e^2)^2/m_N b^2 v^2 . \tag{7.7}$$

If we assume that only the protons and neutrons in ^{9}Li participate in these vibrations ($N = 6$, $Z = 3$), one finds $E^* = 0.26$ MeV in a collision with $b = 15$ fm for ^{11}Li beams (0.8 GeV/nucleon) incident on Pb. This energy is far below the excitation energy of giant dipole resonances (GDR) in normal nuclei, which means that the excitation cross section of a giant dipole mode in the ^{9}Li core is small.

Indeed, assuming that this dipole resonance excited on the ^{9}Li core can be accounted for in the same way as a normal giant dipole resonance positioned at E_{GR}, and using the TRK sum rule, one finds for the total Coulomb cross section

$$\sigma_{GR} = \frac{2}{\pi} Z_T^2 \alpha \left(\frac{c}{v}\right)^2 \frac{\mathrm{SR}}{E_{GR}(\mathrm{MeV})} \left(\xi K_0 K_1 - \frac{v^2 \xi^2}{2c^2}(K_1^2 - K_0^2)\right) \mathrm{mb} , \tag{7.8a}$$

$$\mathrm{SR} = 60NZ/A , \tag{7.8b}$$

where all modified Bessel functions, K_n, are functions of $\xi = E_{GR}R/\gamma\hbar v$, and N, Z and A refer to the neutron, charge and mass number of the ^{9}Li core (6, 3 and 9, respectively). Assuming that the resonance lies in the energy range $E_{GR} = 10$–20 MeV, and for beams with 0.8 GeV/nucleon incident on Pb, one finds $\sigma_{GR} \simeq 50$–400 mb.

One could think about other vibrational modes in ^{11}Li, like all protons vibrating against all neutrons, or a ^{9}Li core vibrating against the di-neutron system. (Such type of motion has been recently studied by Suzuki et al. [56], which is called by the authors a *pygmy* resonance.) For the former case ($N = 8$, $Z = 3$ and $A = 11$) we find $E^* = 0.29$ MeV, while for the latter case one makes the substitution of Z by $Z^2/(A-2)$ in the equation for ΔE_1 and obtains $E^* = 0.02$ MeV. From these values one sees that it is very improbable that the latter vibrational mode could be excited. It is much more reasonable to think that another possible way for the ^{11}Li to absorb energy is by the excitation of vibrations of all protons against all neutrons in it. Due to the existence of the neutron halo, one might think that the protons

move almost freely inside ^{11}Li and that the excitation of such dipole vibrations will occur at very small energies (soft dipole mode).

Recently, Kobayashi et al. [57] have measured the total cross section for the dissociation of ^{11}Li (into ^{9}Li + 2n) incident on several targets (Pb, Cu and C) with beams of 0.8 GeV/nucleon. We shall refer to their particular result for Pb targets which has the advantage of having a large Z, and induces a large Coulomb cross section. They obtained the value $\sigma_C = 1.31 \pm 0.13$ b. In the ^{9}Li + 2n cluster model, the total cross section for direct Coulomb dissociation is obtained by an integration of (6.6) which results in

$$\sigma_{CD} = \tfrac{4}{3}\pi Z_T^2 \alpha^2 \left(\frac{c}{v}\right)^2 \left(\frac{Z_1 A_2 - A_1 Z_2}{A}\right)^2 \frac{1}{\eta^2} \left(\ln\left(\frac{\gamma\hbar v}{\delta\varepsilon R}\right) - \frac{v^2}{2c^2}\right). \tag{7.9}$$

For the reaction cited above it gives $\sigma_{CD} \simeq 1.44^{+2.9}_{-0.7}$ b, where the uncertainties are due to the error in the binding energy.

The nuclear contribution to the direct break-up cannot be obtained by an integration of (7.5) because it was based on the impulse approximation, neglecting the interference with an eclipse term. Including such an effect the cross section is well described by the Glauber formula [58]

$$\sigma_{ND} = \tfrac{1}{6}\pi(2\ln 2 - \tfrac{1}{2})R_T/\eta\,. \tag{7.10}$$

In addition to this (diffractional) dissociation one has to account for the absorption of the 2n system by the target (stripping). The cross section for this process was obtained for the deuteron by Serber [59]. For other cluster-like $[a + (A - a)]$ nuclei one has

$$\sigma_{NS} = \tfrac{1}{2}\pi(a/A)R_T/\eta\,. \tag{7.11}$$

For the reaction ^{11}Li + target$\rightarrow$ ^{9}Li + X one obtains $\sigma_{ND} = 270^{+100}_{-53}$ mb and $\sigma_{NS} = 165^{+63}_{-32}$ mb, respectively. One then sees that the Coulomb dissociation accounts for the main part of the measured cross section, although the nuclear contribution is not negligible. At this point we observe that the Coulomb–nuclear interference in these reactions may be neglected for the following reason. The nuclear contribution to the total cross section can at most come from those impact parameters (from b_{min} to b_{max}) for which the neutron halo of ^{11}Li touches the nuclear matter distribution of Pb. The contribution of the Coulomb field to the total cross section from this interval of impact parameters is, percentually, given by

$$\Delta = \frac{\ln(b_{max}/b_{min})}{\ln(\gamma\hbar v/\delta\varepsilon b_{min})}\,. \tag{7.12}$$

Using typical values of $b_{min} \simeq 10$ fm and $b_{max} \simeq 13$ fm, one finds $\Delta \simeq 5\%$. This means that only about 5% of the Coulomb contribution should interfere with the nuclear contribution. The reason is that, although the fragmentation induced by the Coulomb interaction may be small in a single collision, the interval of impact parameters contributing to the total cross section is very large, up to some hundreds of fermis. Therefore, we can write $\sigma_{total} \simeq \sigma_N + \sigma_C$. Adding the Coulomb dissociation, the nuclear diffraction dissociation, and the stripping cross sections one can reproduce quite well the experimental value of Kobayashi et al. [57] for the total cross sections for two-neutron removal from secondary beams of ^{11}Li incident on Pb.

If we now restrict our study to the Coulomb contribution to the dissociation, which is the dominant part of the cross sections, we find that the excitation of giant resonances as described above can also lead to large values of the cross sections. In fact, if we assume that the energy of excitation, E_{GR}, of a soft vibration mode in ^{11}Li is of the order of 1 MeV, and that the contribution of this soft mode to the sum rule SR is of about 10%, we find (using $N=8$, $Z=3$ and $A=11$) $\sigma_{GR} \simeq 1.3$ b. Due to its low binding energy, one of the main channels for the decay of this resonance must be the emission of the two neutrons. This indicates that the excitation of this soft dipole mode is another possible mechanism to explain the narrow momentum component in the data for $^{11}\text{Li} \rightarrow {}^{9}\text{Li} + \text{X}$, as well as the total cross section for the fragmentation.

From the present available data it does not seem possible to find out whether the fragmentation $^{11}\text{Li} \rightarrow {}^{9}\text{Li} + \text{X}$ in secondary beam reactions proceeds via the direct break-up of a two-cluster system or by the excitation of a soft dipole mode. But note that the two mechanisms assume very distinct structures for ^{11}Li. The direct break-up supposes that the protons are tightly bound to the neutrons in the ^{9}Li core, while the excitation of the soft mode assumes that the protons move almost freely against a neutronic background. Since the Coulomb kick to the protons does not enter in either hypothesis, only one of the two mechanisms could be responsible for the measured cross sections. Due to the large errors in the knowledge of the binding energy of two neutrons in ^{11}Li, and also due to lack of information about the energy location and about the strength of the photonuclear cross section for ^{11}Li at the energies involved, precise theoretical calculations based on either of these models are not conclusive, and the agreement with the experimental data is not unique. Certainly, more experimental results and theoretical discussions are needed in order to determine which of the nuclear models is adequate.

In contrast to the simple models described above, conventional shell-model calculations performed by Bertsch and collaborators [61, 62] have been unable to reproduce the amount of electric dipole strength in ^{11}Li necessary to explain the electromagnetic dissociation cross sections. As concluded by Bertsch and Foxwell [61] it may be essential to take cluster aspects into account. Nonetheless, the failure of the shell-model calculations to determine the enhancement of the electric dipole strength of ^{11}Li at low energies – which is needed to reproduce the experimental data – has led those authors to wonder whether the experimental values of the electromagnetic dissociation cross sections [57] have been correctly extracted from the total cross sections.

Their point is that in ref. [57] one assumes that the nuclear cross section scales as $\sigma_N = 2\pi(R_P + R_T)\Delta$, which is characteristic of a peripheral process concentrated in a small ring width Δ at the surface of the projectile (Serber model). By adjusting the parameters of this scaling law the "experimental" values of σ_N were obtained for other targets, and the Coulomb contribution σ_C to the cross section was inferred by subtraction. But, since ^{11}Li has a long tail in its matter distribution, such a procedure is doubltful. Assuming that the target is a "black disk", the nuclear stripping of the outer nucleons in ^{11}Li should be

$$\sigma_N = 2\pi(R_P + R_T)\Delta P(R_T)\,, \tag{7.13}$$

where $P(R_T)$ is the probability that the outer neutrons will be removed from ^{11}Li. Due to the long matter tail, this probability depends on R_T. Actually it should be approximately proportional to the area A of overlap between the target and the neutron halo in ^{11}Li. From simple geometrical considerations it is possible to show that $A \propto R_T$. That is, σ_N should increase like R_T^2, which would result in larger values of σ_N^{exp} than what was determined in ref. [57]. This has as a consequence that σ_C^{exp}

should be smaller than the values determined by Kobayashi et al. [57]. Indeed, in ref. [63] an eikonal approach to the nuclear dissociation of ^{11}Li using the nucleon–nucleon amplitudes as input has shown that a more appropriate parametrization of σ_N and A_T is

$$\sigma_N = (aA_T^{1/3} + bA_T^{2/3} + c)\,\text{mb}\,, \tag{7.13a}$$

$$a = 98.7\,, \qquad b = 2.284\,, \qquad c = -25.89\,. \tag{7.13b}$$

For large values of A_T, the above equation results in an appreciable deviation from the $A_T^{1/3}$ scaling law [57]. This is in fact a very relevant point since the electromagnetic dissociation of neutron-rich nuclei reveals important aspects of their intrinsic structure.

8. Conclusions

It is quite obvious from our results presented in the previous chapters, that the $t\rho_1\rho_2$ interaction, corrected for by Pauli blocking and higher-order multiple-scattering effects, is only adequate for accounting for the absorptive content of the HI interaction, in a limited energy domain, contrary to several claims [2]. This energy region is dominated by single- and/or double-nucleon knockout processes. At lower energies the Pauli blocking, though slightly weakened by the attractive nuclear interaction, reduces significantly the contribution of these processes to the total reaction cross section. This is also the conclusion reached when a nuclear-matter G-matrix calculation is performed [4].

To account for σ_R at $E/A < \varepsilon_F$, several channels, related principally to mean field effects, such as fusion, incomplete fusion, deep inelastic, nuclear quasi-elastic and particle transfer channels, have to be added to the knockout channel. This has been partially carried out by Faessler [4]. At relativistic energies, peripheral processes play a relevant role, and Coulomb excitation of giant resonances (or direct Coulomb fragmentation) dominates the reaction cross section, especially for loosely bound nuclei.

Appendix A. Derivation of σ_R from the Wronskian

In this appendix, we supply a derivation of σ_R using explicitly the optical Schrodinger equation

$$-(\hbar^2/2\mu)\nabla^2\psi^{(+)} + (V - \mathrm{i}W)\psi^{(+)} = E\psi^{(+)}\,, \tag{A.1}$$

where we take $W > 0$ to describe absorption. From (A.1) one can immediately derive the equation for flux conservation,

$$\hbar \int \nabla\cdot j\,\mathrm{d}^3r = 2\langle\psi^{(+)}|W|\psi^{(+)}\rangle\,, \tag{A.2}$$

where j is the probability current

$$j = (\hbar/2\pi\mathrm{i})[\psi^*\nabla\psi - (\nabla\psi^*)\psi]\,. \tag{A.3}$$

Applying Gauss' theorem to the lhs (A.2), we have then

$$-\int \boldsymbol{j}\cdot \mathrm{d}\boldsymbol{A} = (2/\hbar)\langle \psi^{(+)}|W|\psi^{(+)}\rangle \,, \tag{A.4}$$

where the integral is over any surface surrounding the interaction, in a region where the potential has vanished. Equation (A.4) simply says that the net radial flux is not zero because of absorption. The total reaction cross section is defined as the net inward radial flux given by the lhs of (A.4) divided by the incident flux $|\psi^{(+)}|^2 v$, where v is the asymptotic relative velocity

$$\sigma_{\mathrm{R}} = \frac{-\int \boldsymbol{j}\cdot \mathrm{d}\boldsymbol{A}}{|\psi^{(+)}|^2 v} = \frac{2}{\hbar v}\,\frac{\langle \psi^{(+)}|W|\psi^{(+)}\rangle}{|\psi^{(+)}|^2} \,. \tag{A.5}$$

If we choose the normalization of $\psi^{(+)}$ to be $|\psi^{(+)}|^2 = 1$ we obtain our expression for σ_{R}, eq. (2.9),

$$\sigma_{\mathrm{R}} = (2/\hbar v)\langle \psi^{(+)}|W|\psi^{(+)}\rangle = (k/E)\langle \psi^{(+)}|W|\psi^{(+)}\rangle \,. \tag{A.6}$$

We leave it to the reader to convince himself that eq. (A.4) can be written in the more familiar optical theorem form,

$$\frac{4\pi}{k}\,\mathrm{Im}\, f(0) - \int |f(\theta)|^2\, \mathrm{d}\Omega = \frac{k}{E}\,\langle \psi^{(+)}|W|\psi^{(+)}\rangle \,, \tag{A.7}$$

where the first term is the total cross section and the second the total elastic cross section. Clearly (A.6) is consistent with (A.7).

The extention of the above considerations to coupled channels is straightforward. Instead of eq. (A.1) we now have to consider the following:

$$-\frac{\hbar}{2\mu}\nabla^2\psi_0^{(+)} + (V_0 - \mathrm{i}W_0)\psi_0^{(+)} = E\psi_0^{(+)} - \sum_{j\neq 0} V_{0j}\psi_j^{(+)} \,, \tag{A.8}$$

where W_0 represents the absorptive potential in $|\psi_0^{(+)}\rangle$, in the limit $V_{0j} = 0$.

Gauss' theorem then gives

$$-\int \boldsymbol{j}\cdot \mathrm{d}\boldsymbol{A} = \frac{2}{\hbar}\,\langle \psi_0^{(+)}|W|\psi_0^{(+)}\rangle + \frac{2}{\hbar}\,\mathrm{Im}\langle \psi_0^{(+)}|V_{0j}G_j^{(+)}V_{j0}|\psi_0^{(+)}\rangle \,. \tag{A.9}$$

The second term on the left-hand side represents the contribution to $\int \boldsymbol{j}\cdot \mathrm{d}\boldsymbol{A}$ arising from the channels j, coupled to the entrance channel. This term can be further decomposed, as was shown in chapter 2, into a genuine open-channels contribution and closed-channels contributions (fusion). In fact, taking V_{0j} to be Hermitian, we have [19]

$$\begin{aligned}
\mathrm{Im}\langle \psi_0^{(+)}|V_{0j}G_j^{(+)}V_{j0}|\psi_0^{(+)}\rangle &= \langle \psi_0^{(+)}|V_{0j}\,\mathrm{Im}\, G_j^{(+)}V_{j0}|\psi_0^{(+)}\rangle \\
&= \sum_j \langle \psi_0^{(+)}|V_{0j}(-\pi|\psi_j^{(-)}\rangle\langle \psi_j^{(-)})|V_{j0}|\psi_0^{(+)}\rangle \\
&\quad - \langle \psi_0^{(+)}|V_{0j}G_j^{(+)\dagger}W_jG_j^{(+)}V_{j0}|\psi_0^{(+)}\rangle \\
&= -\pi\int |\langle \psi_j^{(-)}|V_{j0}|\psi_0^{(+)}\rangle|^2\, \mathrm{d}\Omega_j - \sum_j \langle \psi_j^{(+)}|W_j|\psi_j^{(+)}\rangle \,.
\end{aligned} \tag{A.10}$$

Accordingly, (A.6) becomes now

$$\sigma_{\rm R} = \frac{k}{E}\left(\langle\psi_0^{(+)}|W_0|\psi_0^{(+)}\rangle + \sum_{j\neq 0}\langle\psi_j^{(+)}|W_j|\psi_j^{(+)}\rangle\right) + \sigma_{\rm D}\,, \tag{A.11}$$

where $\sigma_{\rm D}$ describes the direct-channels contribution.

Appendix B. Comparison between $\delta_{\rm I}^{\rm (WKB)}$ and $\delta_{\rm I}^{\rm (eikonal)}$

In this short appendix we present a comparison between the imaginary part of the nuclear elastic phase shift calculated within the eikonal approximation, eq. (2.22),

$$\delta_{\rm I}^{\rm (E)}(b) = -\frac{1}{4}\frac{2\pi}{\hbar^2 k}\int_{-\infty}^{\infty} {\rm d}z\, W(\sqrt{b^2+z^2})\,, \tag{B.1}$$

with the more precise one obtained within the WKB approximation, eq. (2.19),

$$\begin{aligned}\delta_{\rm I} &= \frac{2\mu}{\hbar^2}\int_{r_1}^{\infty} {\rm d}r'\left[\left(E - \frac{Eb^2}{r'^2} - U(r')\right)^2 + W^2(r')\right]^{1/4}\sin[\tfrac{1}{2}\theta(r')]\,,\\ \tan\theta(r') &= -W(r')[E - Eb^2/r'^2 - U(r')]^{-1}\,,\end{aligned} \tag{B.2}$$

for several cases, involving the $^{12}{\rm C} + {}^{12}{\rm C}$ system, using $U(r') = 0$ for simplicity. A Woods–Saxon form was employed for $W(r')$,

$$W(r) = -W_0[1 + \exp(r - R_0/a)]^{-1}\,, \tag{B.3}$$

with $a = 0.6$ fm and $R_0 = 8.0$ fm. W_0 was varied.

The results are presented in fig. 28. Clearly, the higher the energy, the better the agreement one obtains between the two expressions. In the application described in this paper, we have always employed the WKB expression with the real part of the potential taken into account.

Appendix C. Pauli blocking effects on the nucleus–nucleus total cross section

C.1. Calculation of $\bar{\sigma}_{\rm NN}$ for nucleon–nucleus scattering

In the first part of this appendix, we review the calculation of $\bar{\sigma}_{\rm NN}$ in nucleon–nucleus scattering. Although this has been discussed extensively by several authors, we feel that a review is necessary as a preparation for the calculation of $\bar{\sigma}_{\rm NN}$ in the nucleus–nucleus case, presented in the second part of this appendix.

The average cross section of two nuclei, one of which is found with momentum $\boldsymbol{k}_2$ is given by

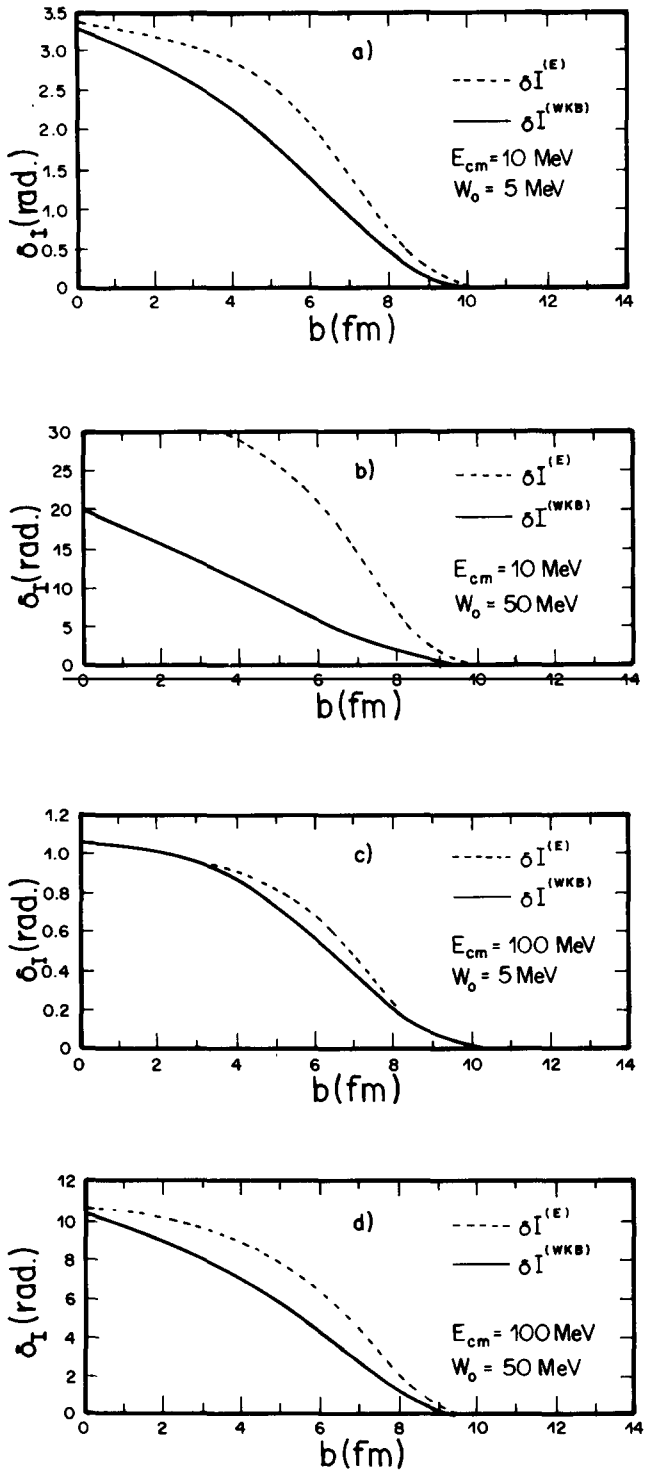

Fig. 28. The imaginary phase shift calculated according to the WKB approximation (solid curve) and the eikonal approximation (dashed curve): (a) $E_{CM} = 10$ MeV, $W_0 = 5$ MeV; (b) $E_{CM} = 10$ MeV, $W_0 = 50$ MeV; (c) $E_{CM} = 100$ MeV, $W_0 = 5$ MeV; (d) $E_{CM} = 100$ MeV, $W_0 = 50$ MeV.

$$\bar{\sigma} = \frac{1}{V_{F2}} \int_{V_{F2}} d\boldsymbol{k}_2 \, \sigma_T^{NN}(\boldsymbol{q}, \boldsymbol{q}') , \tag{C.1}$$

where $V_{F2} \equiv \frac{4}{3}\pi k_{F2}^3$ is the volume of the Fermi sphere representing the target nucleus (labeled here by 2), and $\sigma_T^{NN}(\boldsymbol{q}, \boldsymbol{q}')$ is the free nucleon–nucleon cross section, which depends on the relative momenta $\boldsymbol{q} = \boldsymbol{k}_1 - \boldsymbol{k}_2$ and $\boldsymbol{q}' = \boldsymbol{k}_1' - \boldsymbol{k}_2'$, before and after the collision, respectively, where $\boldsymbol{k}_1$ is the incident nucleon momentum. When using eq. (4.1) one normally employs for σ_T^{NN} an empirical form, which is valid for fixed target nucleons. To correct for this, namely for the fact that $\boldsymbol{k} \neq 0$, one inserts a transformation factor, $|\boldsymbol{k}_1 - \boldsymbol{k}_2|/k_1$, thus giving

$$\bar{\sigma} = \frac{1}{V_{F2}} \int d\boldsymbol{k}_2 \, \frac{|\boldsymbol{k}_1 - \boldsymbol{k}_2|}{k_1} \, \sigma_T^{NN} . \tag{C.2}$$

Clearly, Pauli blocking enters through the restriction, $|\boldsymbol{k}_1'| > k_{F2}$, $|\boldsymbol{k}_2'| > k_{F2}$. Therefore, when expressed in terms of the differential cross section, eq. (C.2) takes the following form in the energy region, where $\sigma^T = \int d\Omega \, d\sigma/d\Omega$:

$$\bar{\sigma} = \frac{1}{V_{F2}} \int d\boldsymbol{k}_2 \, \frac{|\boldsymbol{k}_1 - \boldsymbol{k}_2|}{k_1} \int d\Omega \, \frac{d\sigma}{d\Omega} \quad \text{for } k_1'^2 + k_2'^2 > 2k_{F2}^2 . \tag{C.3}$$

Using now energy and momentum conservation, we can recast the above equation into the following form:

$$\sigma_1 = \frac{1}{V_{F2}} \int d\boldsymbol{k}_2 \, \frac{|\boldsymbol{k}_1 - \boldsymbol{k}_2|}{k_1} \int_{k_1'^2 + k_2'^2 > 2k_{F2}^2}^{k_1'^2 + k_2'^2 = k_1^2 + k_2^2} d\Omega \, \delta(\boldsymbol{q} - \boldsymbol{q}') \, d\boldsymbol{q}' \, \frac{d\sigma}{d\Omega} . \tag{C.4}$$

After integrating over $\boldsymbol{q}'$, we obtain, assuming $d\sigma/d\Omega = \sigma_T^{NN}(q)/4\pi$, the following

$$\bar{\sigma} = \frac{1}{k_1 V_{F2}} \int d\boldsymbol{k}_2 \, \frac{|k_2^2 + k_1^2 - 2k_{F2}^2|}{|\boldsymbol{k}_1 + \boldsymbol{k}_2|} \, \sigma_T^{NN}(q) , \tag{C.5}$$

where the lower limit of integration, obeys, $k_1^2 + k_2^2 > 2k_{F2}$.

It is usual practice to assume that $\sigma_T^{NN}(q)$ is a constant, σ_0, which results in the following simple expression for $\bar{\sigma}_{NN}$:

$$\bar{\sigma} = \begin{cases} \sigma_0[1 - \frac{7}{5}(k_{F2}^2/k_1^2)] , & k_1^2 \geq 2k_{F2}^2 , \\ \sigma_0[1 - \frac{7}{5}(k_{F2}^2/k_1^2) + \frac{2}{5}(k_{F2}^2/k_1^2)(2 - k_1^2/k_{F2}^2)^{5/2}] , & k_1^2 \leq 2k_{F2}^2 , \end{cases} \tag{C.6}$$

which are nothing but eqs. (4.3), (4.4), mentioned in section 4.

In the application we envisage in this paper, we shall use the empirical energy-dependent $\sigma_T^{NN}(q)$. For this purpose, a more convenient form for the evaluation of $\bar{\sigma}_{NN}$ is the following, equivalent, relation:

$$\bar{\sigma} = \frac{1}{k_1 V_{F2}} \int d\boldsymbol{k}_2 \, |\boldsymbol{k}_1 - \boldsymbol{k}_2| \, \frac{\sigma_T^{NN}(q)}{4\pi} \int_{\text{Pauli}} d\Omega \,, \tag{C.7}$$

where the restrictions imposed by the conservation laws and Pauli's principle are contained implicitly in the solid-angle integral. The above form of $\bar{\sigma}_{NN}$ is the one which is most easily adaptable to the ion–ion case.

In the calculation of the integral $\int_{\text{Pauli}} d\Omega$, one resorts to geometrical arguments. Pauli blocking, within the Fermi gas model used here, implies a restriction on the lengths of the vectors $\boldsymbol{k}_1'$ and $\boldsymbol{k}_2'$, as visualized in fig. 29a. The momenta $\boldsymbol{k}_1$ and $\boldsymbol{k}_2$ define the total momentum $2\boldsymbol{p} = \boldsymbol{k}_1 + \boldsymbol{k}_2$ and the relative momentum $2\boldsymbol{q} = \boldsymbol{k}_1 - \boldsymbol{k}_2$, with $\boldsymbol{p}$ specifying the center of the scattering sphere and $\boldsymbol{q}$ it radius, as indicated in fig. 29b; the conservation of linear momentum implies fixed $\boldsymbol{p}$. From energy conservation, we also have $\boldsymbol{k}_1 \cdot \boldsymbol{k}_2 = \boldsymbol{k}_1' \cdot \boldsymbol{k}_2'$ and $\boldsymbol{q} = \boldsymbol{q}'$, which implies a constant radius for the scattering sphere. Imposing now Pauli blocking, gives

$$|\boldsymbol{k}_1'| = |\boldsymbol{p} + \boldsymbol{q}'| > k_{F2} \,, \qquad |\boldsymbol{k}_2'| = |\boldsymbol{p} - \boldsymbol{q}'| > k_{F2} \,, \tag{C.8}$$

which implies that the amount of solid angle not allowed is as indicated in fig. 29c by the dashed area.

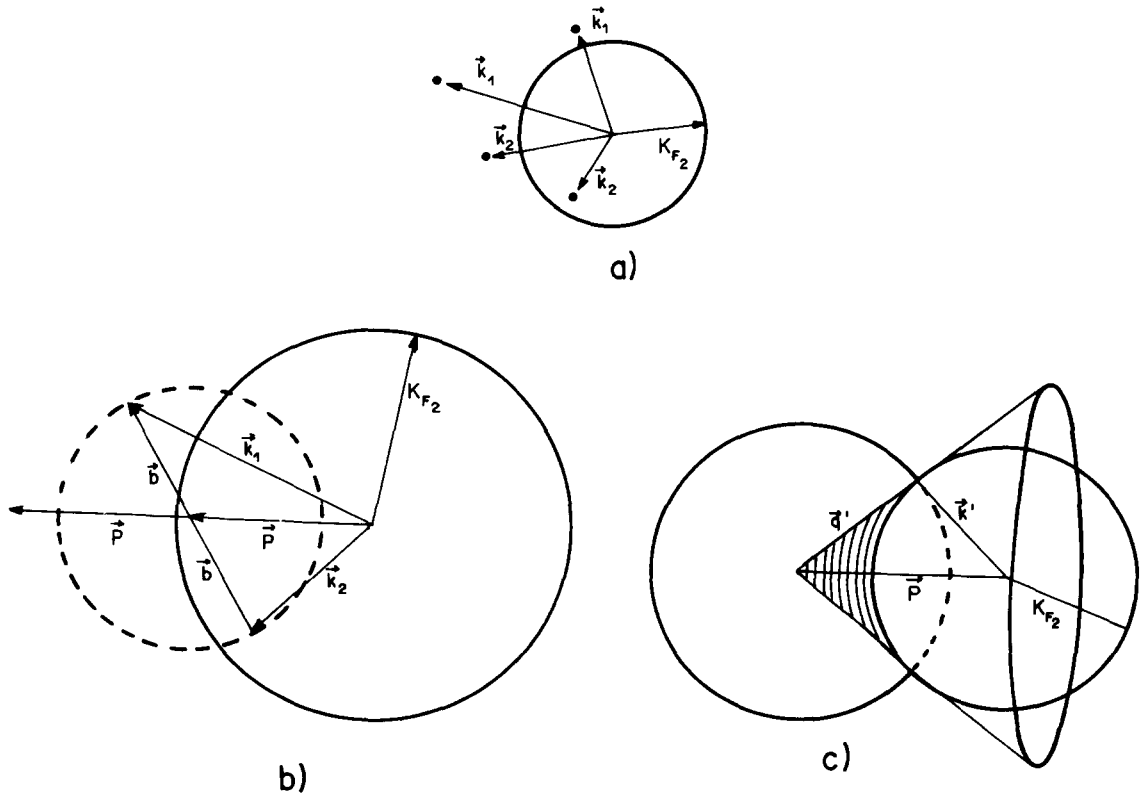

Fig. 29. The geometrical realization of Pauli blocking in the nucleon–nucleus system: (a) restrictions on the momentum vectors; (b) the allowed scattering sphere and (c) the Pauli forbidden region (dashed area).

Thus $\int_{\text{Pauli}} d\Omega = 4\pi - \Omega_a$, which when inserted in eq. (C.7), yields the closed expression, eq. (C.6), if a constant $\sigma_T^{NN}(q)$ is used. The solid angle portion Ω_a is given by [obtained directly from eq. (C.8)]

$$\Omega_a = 4\pi - 2\pi(k_1^2 + k_2^2 - 2k_{F2}^2)/2q \cdot 2p \,. \tag{C.9}$$

C.2. Calculation of $\bar{\sigma}_{NN}(E)$ for nucleus–nucleus scattering

In the nucleus–nucleus case, the calculation of $\bar{\sigma}_{NN}(E)$ involves the considerations of three spheres; the two Fermi spheres representing the projectile and target nuclei and the scattering sphere, determined by the momentum and energy conservation laws and the Pauli principle, in close analogy with the considerations presented in the first part of this appendix.

The starting expression of $\bar{\sigma}_{NN}(E)$ in the nucleus–nucleus case is

$$\bar{\sigma}_{NN}(k, k_{F1}, k_{F2}) = \frac{1}{V_{F1}V_{F2}} \int d\boldsymbol{k}_1\, d\boldsymbol{k}_2\, \frac{2q}{k}\, \frac{\sigma_T^{NN}(q)}{4\pi} \int_{\text{Pauli}} d\Omega \,, \tag{C.10}$$

where $V_{F1} = \frac{4}{3}\pi k_{F1}^3$ and $V_{F2} = \frac{4}{3}\pi k_{F2}^2$ are the Fermi volumes of the projectile and target nuclei, respectively, and $2q = |\boldsymbol{k}_1 - \boldsymbol{k}_2 + \boldsymbol{k}|$ with k denoting the relative-momentum spheres alluded to above. Using similar arguments as those discussed in the first part of this appendix, leads us to conclude that the region *not* allowed by the Pauli exclusion principle in the nucleus–nucleus case is the one shown as the shaded region in fig. 30b.

The restricted solid-angle integral is

$$\int_{\text{Pauli}} d\Omega = \Omega_{\text{Pauli}}(\theta_a, \theta_b, \theta) = 4\pi - 2\Omega_a - 2\Omega_b + \bar{\Omega} \,, \tag{C.11}$$

where Ω_a and Ω_b are the solid angles specifying the excluded cones and $\bar{\Omega}$ represents the intersection area of the two conical sections. The solid angles Ω_a and Ω_b are easily determined.

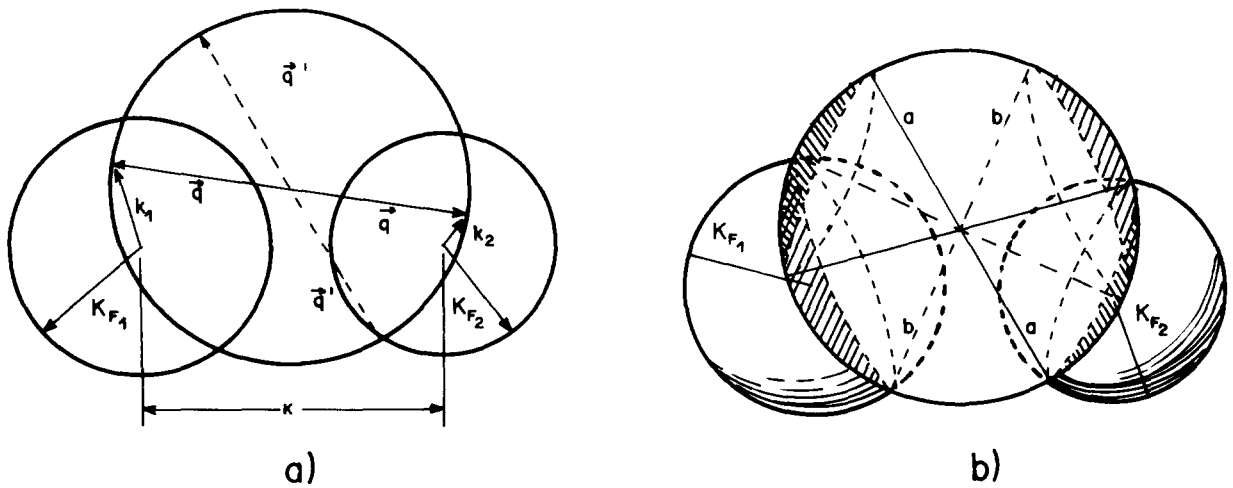

Fig. 30. Same as fig. 29 for the nucleus–nucleus system: (a) the three "spheres" describing the scattering region in momentum space, and (b) the Pauli forbidden region (dashed area).

$$\Omega_a = 2\pi(1-\cos\theta_a)\,, \qquad \Omega_b = 2\pi(1-\cos\theta_b)\,, \tag{C.12}$$

$$\cos\theta_a = (p^2+q^2-k_{\mathrm{F2}}^2)/2pq\,, \qquad \cos\theta_b = (p^2+q^2-k_{\mathrm{F1}}^2)/2bq\,, \tag{C.13}$$

$$2\boldsymbol{p} = \boldsymbol{k}_2 + \boldsymbol{k} + \boldsymbol{k}_1\,, \qquad 2\boldsymbol{q} = \boldsymbol{k}_2 - \boldsymbol{k} - \boldsymbol{k}_1\,, \qquad \boldsymbol{b} = \boldsymbol{k} - \boldsymbol{p}\,. \tag{C.14}$$

The evaluation of $\bar{\Omega}$ is tedious but straightforward [60]. We give below the pertinent expressions. Two possibilities arise:

(1) $\bar{\Omega} = 2\Omega_i(\theta, \theta_a, \theta_b) + 2\Omega_i'(\pi-\theta, \theta_a, \theta_b)$ for $\theta + \theta_a + \theta_b > \pi$, (C.15)

(2) $\bar{\Omega} = 2\Omega_i(\theta, \theta_a, \theta_b)$ for $\theta + \theta_a + \theta_b \le \pi$, (C.16)

where the angle θ is given by

$$\cos\theta = (k^2 - p^2 - b^2)/2pb\,. \tag{C.17}$$

The solid angle Ω_i has the following values:

(a) $\Omega_i = 0$ for $\theta \ge \theta_a + \theta_b$, (C.18)

(b)
$$\Omega_i = 2\Bigg[\cos^{-1}\left(\frac{\cos\theta_b - \cos\theta\cos\theta_a}{\sin\theta_a\,(\cos^2\theta_a + \cos^2\theta_b - 2\cos\theta\cos\theta_a\cos\theta_b)^{1/2}}\right)$$
$$+ \cos^{-1}\left(\frac{\cos\theta_a - \cos\theta\cos\theta_b}{\sin\theta_b(\cos^2\theta_a + \cos^2\theta_b - 2\cos\theta\cos\theta_a\cos\theta_b)^{1/2}}\right)$$
$$- \cos\theta_a\cos^{-1}\left(\frac{\cos\theta_b - \cos\theta\cos\theta_a}{\sin\theta\sin\theta_a}\right) - \cos\theta_b\cos^{-1}\left(\frac{\cos\theta_a - \cos\theta\cos\theta_b}{\sin\theta\sin\theta_b}\right)\Bigg]\,,$$

for $|\theta_b - \theta_a| \le \theta \le \theta_a + \theta_b$, (C.19)

(c) $\Omega_i = \Omega_b$ for $\theta_b \le \theta_a$, $\theta \le |\theta_b - \theta_a|$, (C.20)

(d) $\Omega_i = \Omega_a$ for $\theta_a \le \theta_b$, $\theta \le |\theta_b - \theta_a|$. (C.21)

The first case above represents the situation where no intersection of the two conic sections, a and b, occurs.

We should mention that in some cases, for several values of p, q and k_{F1}, the cosine functions above may happen to attain unphysical values (>1). These cases are

(1) $p + q < k_{\mathrm{F2}}$ for $\cos\theta_a < -1$,

(2) $|p+q| > k_{\mathrm{F2}}$ for $\cos\theta_a > +1$,

(3) $p + q < k_{\mathrm{F1}}$ for $\cos\theta_b < -1$, (C.22)

(4) $|p-q| > k_{\mathrm{F1}}$ for $\cos\theta_b > 1$.

Under conditions 1 and 3 we merely set $\int_{\text{Pauli}} d\Omega$ equal to zero, since the scattering sphere in this case is situated inside the Fermi sphere of either the target or projectile nucleus. If, on the other hand, $\cos\theta_a > 1$ and $\cos\theta_b > 1$ (conditions 2 and 4) then two possibilities are considered,

$$|p-q| > k_{F2}\,, \quad \begin{cases} p > q \rightarrow \Omega_a = 0\,, \\ p < q \rightarrow \Omega_{\text{Pauli}}(\theta_a, \theta_b, \theta) = 0\,, \end{cases} \tag{C.23}$$

$$|b-q| > k_{F1}\,, \quad \begin{cases} b > q \rightarrow \Omega_b = 0\,, \\ b < q \rightarrow \Omega_{\text{Pauli}}(\theta_a, \theta_b, \theta) = 0\,. \end{cases} \tag{C.24}$$

The cases $\Omega_a = 0$ and $\Omega_b = 0$ represent the situations when the scattering sphere does not intersect the Fermi spheres.

In eq. (C.10) the average nucleon–nucleon cross section $\bar{\sigma}_{NN}$ clearly depends on the Fermi momenta k_{F1} and k_{F2} which are related to the matter densities according to [32]

$$k_F^2(r) = \left[\tfrac{3}{2}\pi^2\rho(r)\right]^{2/3} + \tfrac{5}{2}\xi\left[(\nabla\rho)/\rho\right]^2\,, \tag{C.25}$$

where the second term amounts to a surface correction with ξ about 0.1.

In our calculastion of $\bar{\sigma}_{NN}$, we have used the above expression for k_{F1} and k_{F2} in eq. (C.10), which was evaluated numerically. A simple analytic expression, such as given in eq. (3.3) for the nucleon–nucleus case, was found, even in the limiting case of the constant free nucleon–nucleon total cross section.

References

[1] P.J. Karol, Phys. Rev. C 11 (1975) 1203.

[2] R.M. de Vries and J.C. Peng, Phys. Rev. C 22 (1980) 1055;
see also N.J. Di Giacomo and R.M. de Vries, Comments Nucl. Part. Phys. 12 (1984) 111.

[3] D.M. Brink and R.G. Satchler, J. Phys. G 7 (1981) 43.

[4] A. Faessler, L. Rikus and S.B. Khadkibar, Nucl. Phys. A 401 (1983) 157.

[5] J.C. Peng, R.M. de Vries and N.J. Di Giacomo, Phys. Lett. B 96 (1981) 244.

[6] H.B. Bidasaria, L.W. Townsend and J.W. Wilson, J. Phys. G 9 (1983) L17.

[7] M. Buenerd, J. Pinston, J. Cole, C. Guet, D. Lebnen, J.M. Loisseaux, P. Martin, E. Monnand, J. Mougey, H. Nifenecker, R. Ost, P. Perrin, Ch. Ristori, P. de Saintignon, F. Schussler, L. Carlén, H.A. Gusfasson, B. Jakobsson, T. Johansson, G. Jönsson, J. Krumlinde, I. Otterlund, H. Ryde, B. Schröder, G. Tibell, J.B. Bondorf and O.B. Nielsen, Phys. Lett. B 102 (1981) 242; Nucl. Phys. A 424 (1984) 313.

[8] A.J. Cole, W.D.M. Rae, M.E. Brandan, A. Dacal, B.G. Harvey, R. Legrain, M.J. Murphy and R.G. Stokstad, Phys. Rev. Lett. 47 (1981) 1705;
M.E. Brandan, J. Phys. 69 (1983) 197.

[9] C. Perrin, S. Kox, N. Longequeue, J.B. Viano, M. Buenerd, R. Cherkaoui, A.J. Cole, A. Gamp, J. Menet, R. Ost, R. Bertholet, C. Guet and J. Pinston, Phys. Rev. Lett. 49 (1982) 1905;
M. Buenerd et al., Phys. Lett. B 120 (1981) 242;
H.B. Bohlen et al., Z. Phys. A 308 (1982) 121;
S. Kox et al., Phys. Lett. B 159 (1985) 15; Nucl. Phys. A 420 (1984) 162.

[10] R.M. De Vries, N.J. Giacomo, J.S. Kapustinsky, J.C. Peng, W.E. Sondheim, J.W. Sunier, J.G. Gramer, R.E. Loveman, C.R. Gruhn and H.H. Wiemann, Phys. Rev. C 26 (1982) 301.

[11] W.O. Lock and D.F. Measday, Intermediate Energy Nuclear Physics (Menthuen, London, 1970).

[12] See, e.g., P. Braun-Munzinger et al., Phys. Rev. Lett. 52 (1984) 255;
R. Shyam and J. Knoll, in: Nuclei, Proc. Workshop on Coincidence Particle Emission from Continuous States, eds H. Machner and P. Jahn (World Scientific, Singapore, 1984) p. 582.

[13] P.C. Tandy, E.F. Redish and O. Bollé, Phys. Rev. Lett. 35 (1975) 921; Phys. Rev. C 16 (1977) 1924;
D.S. Koltun and D.M. Schneider, Phys. Rev. Lett. 42 (1979) 211.

[14] J.T. Haldemann and R.M. Thaler, Phys. Rev. Lett. 14 (1965) 81; Phys. Rev. 139 (1965) 13186.
[15] M.S. Hussein, H.M. Nussenzveig, A.C.C. Villari and J. Cardoso, Jr, Phys. Lett. B 114 (1982) 1;
see also A.Z. Schwarzchild, E.H. Auerbach, R.C. Fuller and S. Kahana, in: Proc. Symp. on Macroscopic Features of Heavy-Ion Collisions, ANL Report ANL-PHY-76-2.
[16] H. Bethe, Phys. Rev. 57 (1940) 1125;
see also S. Feshbach, R. Serber and T.B. Taylor, Phys. Rev. 75 (1949) 1.
[17] M.M. Shapira, Phys. Rev. 90 (1953) 171.
[18] See, e.g., S.J. Brodsky and J. Pumplin, Phys. Rev. 182 (1968) 1794.
[19] M.S. Hussein, Phys. Rev. C 30 (1984) 1962;
M.S. Hussein, A.J. Baltz and B.V. Carlson, Phys. Rep. 113 (1984) 133.
[20] T. Udagawa and T. Tamura, Phys. Rev. C 29 (1984) 1922;
T. Udagawa, B.T. Kim and T. Tamura, Phys. Rev. C 32 (1985) 124.
[21] M.A. Nagarajan and G.R. Satchler, Phys. Lett. B 173 (1986) 29.
[22] See, e.g., L.G. Arnold and B.C. Clark, Phys. Lett. B 84 (1979) 46;
L.G. Arnold, R.L. Mercer and P. Schwandt, Phys. Rev. C 23 (1981) 1949;
L.G. Arnold, Phys. Rev. C 25 (1982) 936.
[23] B.V. Carlson, M.P. Isidro Filho and M.S. Hussein, Phys. Rev. Lett. 53 (1984) 2222; in: Proc. V. Encontro Nacional de Física de Energias Intermediárias (Gramado, R.S. 1984);
see also, R. Dymarz, Phys. Lett. B 155 (1985) 5.
[24] A.K. Kerman, H. McManus and R.M. Thaler, Ann. Phys. (NY) 8 (1959) 551;
For some reviews see: E.J. Moniz, in: Nuclear Physics with Heavy Ions and Mesons, Les Houches, Session XXX (1977), ed. R. Balian (North-Holland, Amsterdam, 1977);
H. Feshbach, in: Nuclear Physics with Heavy Ions and Mesons, Les Houches, Session XXX (1977) ed. R. Balian (North-Holland, Amsterdam, 1977).
[25] J.M. Eisenberg and D.S. Koltun, Theory of Meson Interactions with Nuclei (Wiley, New York, 1980).
[26] L. Ray, Phys. Rev. C 20 (1979) 1957.
[27] E. Boridy and H. Feshbach, Ann. Phys. (NY) 109 (1977) 468.
[28] G.R. Satchler and W.G. Love, Phys. Rep. 55 (1979) 183.
[29] R.A. Rego and M.S. Hussein, Phys. Rev. C 33 (1986) 2003.
[30] K. Kikuchi and M. Kawai, Nuclear Matter and Nuclear Reactions (North-Holland, Amsterdam, 1968) p. 37.
[31] E. Clementel and C. Villi, Nuovo Cimento II (1955) 176.
[32] See, e.g., B. Sinha, Phys. Rep. 20 (1975) 1; Phys. Rev. Lett. 24 (1982) 209.
[33] B.C. Clark et al., Phys. Rev. Lett. 50 (1983) 1644;
J.R. Shephard, J.A. McNeil and S.J. Wallace, Phys. Rev. Lett. 50 (1983) 1449.
[34] J.A. McNeil, J.R. Shephard and S.J. Wallace, Phys. Rev. Lett. 50 (1983) 1439.
[35] R.D. Amado, J. Piekarewicz, D.A. Sparrow and J.A. McNeil, Phys. Rev. C 28 (1983) 1663.
[36] J. Friar and S.J. Wallace, Phys. Rev. C 28 (1984) 2050.
[37] C.J. Horowitz, Nucl. Phys. A 412 (1984) 228.
[38] T.J. Symons et al., Phys. Rev. Lett. 42 (1979) 40.
[39] G.D. Westfall et al., Phys. Rev. Lett. 43 (1979) 1859.
[40] P.B. Pirce and J. Stevenson, Phys. Rev. C 24 (1981) 2101.
[41] I. Tanihata et al., Phys. Lett. B 160 (1985) 380; Phys. Rev. Lett. 55 (1985) 2676, Phys. Lett. B 206 (1988) 592.
[42] W. Mittig et al., Phys. Rev. Lett. 59 (1987) 1889.
[43] M.G. Saint-Laurent et al., Z. Phys. A 332 (1989) 457.
[44] H. Sato and Y. Okuhara, Phys. Lett. B 162 (1985) 217.
[45] G.F. Bertsch, B.A. Brown and H. Sagawa, Phys. Rev. C 39 (1989) 1154.
[46] J.R. Beene et al., Phys. Rev. C 41 (1990) 920.
[47] C.A. Bertulani and G. Baur, Phys. Rep. 163 (1988) 299.
[48] H. Feshbach and M. Zabek, Ann. Phys. (NY) 107 (1977) 110.
[49] C.A. Bertulani, L.F. Canto, R. Donangelo and J.O. Rasmussen, Mod. Phys. Lett. A 4 (1989) 1315.
[50] C.A. Bertulani and M.S. Hussein, Phys. Rev. Lett. 64 (1990) 1099.
[51] P.G. Hansen and B. Jonson, Europhys. Lett. 4 (1989) 409.
[52] A.S. Goldhaber, Phys. Lett. B 53 (1974) 306.
[53] C.A. Bertulani and G. Baur, Nucl. Phys. A 480 (1988) 615;
G. Baur, in: Proc. Intern. Symp. on Heavy-Ion Physics and Nuclear Astrophysical Problems (Tokyo, July 1988) (World Scientific, Singapore 1989) p. 225.
[54] I. Tanihata, Nucl. Phys. A 478 (1988) 795c.
[55] G. Baur and C.A. Bertulani, Phys. Rev. C 35 (1987) 836.

[56] Y. Suzuki, K. Ikeda and H. Sato, Niigata University, preprint (1989).
[57] T. Kobayashi et al., Phys. Lett. B 232 (1989) 51.
[58] R. Glauber, Phys. Rev. 99 (1955) 1515.
[59] R. Serber, Phys. Rev. 72 (1947) 1008.
[60] C. Bertulani, Rev. Bras. Fís. 16 (1986) 380.
[61] G. Bertsch and J. Foxwell, Phys. Rev. C 41 (1989) 1300, erratum, to be published.
[62] G. Bertsch, E. Esbensen and A. Sustich, Phys. Rev. C 42 (1990) 758.
[63] C.A. Bertulani, G. Baur and M.S. Hussein, Nucl. Phys. A, in press.
[64] S.K. Gupta and S. Kailas, Z. Phys. A 317 (1984) 75.
[65] A. Vitturi and F. Zardi, Phys. Rev. C 36 (1987) 1404.
[66] W. Shen, B. Wang, J. Feng, W. Zhan, Y. Zhu and E. Feng, Nucl. Phys. A 491 (1989) 130.
[67] S.K. Charagi and S.K. Gupta, Phys. Rev. C 41 (1990) 1610.
[68] S. Kox et al., Phys. Rev. C 35 (1987) 1678.
[69] N. Alamos, F. Auger, J. Barrette, B. Berthier, B. Fernandez, J. Gastebois and L. Papineau, Phys. Lett. B 137 (1984) 37.
[70] W. Treu, N. Frohlich, W. Galster, P. Duck and H. Voit, Phys. Rev. C 22 (1980) 2462.
[71] L.W. Townsend and J.W. Wilson, Rad. Res. 106 (1986) 283.